ELSEVIER

Chemical Geology 189 (2002) 105–133

CHEMICAL GEOLOGY
INCLUDING
ISOTOPE GEOSCIENCE

www.elsevier.com/locate/chemgeo

Petrogenesis of syenite–granite suites from the Bryansky Complex (Transbaikalia, Russia): implications for the origin of A-type granitoid magmas

B.A. Litvinovsky [a,b,*], Bor-ming Jahn [c], A.N. Zanvilevich [b], A. Saunders [d], S. Poulain [c], D.V. Kuzmin [e], M.K. Reichow [d], A.V. Titov [e]

[a] *Geological Institute, RAS, Ulan-Ude, Russia*
[b] *Ben-Gurion University of Negev, PO Box 653, Beersheba 84105, Israel*
[c] *Geosciences Rennes, Universite de Rennes 1, 35042 Rennes Cedex, France*
[d] *University of Leicester, Leicester LE1 7RH, UK*
[e] *UIGGM RAS, 3, Koptyug ave, Novosibirsk 670030, Russia*

Received 1 February 2002; accepted 17 June 2002

Abstract

Two syenite–granite suites, metaluminous and peralkaline, that form the Bryansky Complex in Transbaikalia, Russia, have been studied with the aim to constrain the existing models of A-type granitoid magma generation. The Bryansky Complex is a large intrusive body of about 1600 km^2 emplaced in the central part of the Mongolian–Transbaikalian granitoid belt, which extends for more than 2000 km and is 200–300 km wide. The Belt comprises about 350 A-type granitoid plutons and numerous volcanic fields. U–Pb and Rb–Sr isotope dating revealed that all the intrusive rocks of the Complex and closely associated comendites were emplaced within a narrow time span, 279–285 Ma. The isotope characteristics are rather similar for all main rock types. The metaluminous suite has a $(^{87}Sr/^{86}Sr)_T$ value of 0.7050 ± 0.001, $\varepsilon_{Nd}(T)$ from -1.9 to -3.0, and the peralkaline suite has $(^{87}Sr/^{86}Sr)_T = 0.7053 \pm 0.0008$, $\varepsilon_{Nd}(T) = -2.1$ and -2.4. Comendites and trachyandesites have similar $\varepsilon_{Nd}(T)$ values (from -2.2 to -3.5), but a slightly higher $(^{87}Sr/^{86}Sr)_T$ value of 0.7062 ± 0.0002. The systematic change in chemical and mineralogical composition from syenitic to granitic rocks in both suites and the similar isotopic ratios suggest that the granites were formed by fractional crystallization of the syenite magmas. Several lines of evidence suggest that metaluminous syenite is the parental magma for the whole Bryansky Complex. Study of melt inclusions in quartz phenocrysts from the peralkaline granite and in pyroxene from the nordmarkite indicates that fractional crystallization has resulted in significant F enrichment in the granitic magma (up to 1.5–1.7 wt.%). The syenite magmas crystallized at rather high temperature >940 °C whereas the near-liquidus temperature of the peralkaline granite was lower, 760–790 °C. Very high homogenization temperatures of the melt inclusions in quartz phenocrysts from comendites (1000–1100 °C) suggest that the alkali-rich silicic magma formed at a depth of 50–60 km (?) far exceeding the

* Corresponding author. Ben-Gurion University of Negev, P.O. Box 653, Beersheba 84105, Israel. Tel.: +972-8-6477522; fax: +972-8-6472997.

E-mail address: borisl@bgumail.bgu.ac.il (B.A. Litvinovsky).

0009-2541/02/$ - see front matter
PII: S0009-2541(02)00142-0

normal crust thickness. The Sr–Nd isotope data advocate the main role of mantle-derived material in the source region from which the alkali-rich syenitic and granitic magmas were produced.

Keywords: A-type granite; Syenite; Nordmarkite; Comendite origin; Melt inclusions

1. Introduction

The processes giving rise to A-type granitoid magma are fundamental to the evolution and growth of intracontinental crust (e.g., Anderson and Morrison, 1992; Taylor and McLennan, 1995). This type of igneous rocks is observed worldwide. Eby (1990, 1992) distinguished two groups of A-type granites in accordance with their tectonic setting: (1) anorogenic: emplaced during intraplate rifting or as the result of plume or hotspot activity, and (2) postorogenic: emplaced at the end of a long period of apparently high heat flow and granitic magmatism. A number of petrogenetic models have been proposed. The first category of models calls for a predominance of mantle-derived material. They include: (i) fractional crystallization of alkali basalt magma (Loiselle and Wones, 1979; Eby, 1990; Turner et al., 1992), and (ii) minor assimilation of silicic crustal rocks by alkali basalt magma or mixing of basalt magma with crustal-derived silicic melts followed by fractional crystallization processes (Barker et al., 1975; Kerr and Fryer, 1993; Wickham et al., 1995). The second category of models stresses the dominant role of crustal material in the generation of A-type magma: (i) low degrees of melting of F- and Cl-enriched lower crustal granulite residue from which granite melts were previously extracted (Collins et al., 1982; Clemens et al., 1986; Whalen et al., 1987); (ii) melting of tonalitic I-type granites (Anderson and Morrison, 1992; Sylvester, 1989; Creaser et al., 1991; Skjerlie and Johnston, 1992; Patiño Douce, 1997); (iii) melting of lower-crustal source rocks under fluxing of mantle-derived volatiles or metasomatism of granitic magmas (Bailey, 1978; Taylor et al., 1980; Harris et al., 1986). It appears that no single model is suitable for all A-type granitoids from diverse geological setting. The depth of A-type silicic magma generation is also a matter of debate. The hypothesis of magma production in the lower crust is justified by a number of melting experiments (Vielzeuf et al., 1990; Whalen et al., 1987). On the other hand, Patiño Douce (1997) demonstrated that dehydration-melting of calc-alkaline granitoids at pressure ≤ 4 kbar, i.e., in the upper crust, generate silica-rich liquids with the major and trace element features characteristic of A-type granites. By contrast, Litvinovsky et al. (2000) suggested that A-type magma might have formed at great depth that corresponds to the base of overthickened crust or even the uppermost mantle. This is based on data that subduction of silicic crustal material to mantle depths actually occurred (Jahn et al., 1996; Schreyer et al., 1987; Pin and Vielzeuf, 1988; Black et al., 1988; Litvinovsky et al., 2000 and references therein; Del Lama et al., 2000). If deeply subducted crustal blocks were underplated by basalt magma, the silicic material would be melted when the temperature is sufficiently high, about 950–1000 °C (Stern et al., 1975). There is evidence that such temperatures were attained in some high-pressure granulite terranes (about 12–14 kbar) in which partial melting also occurred (Hayob et al., 1989; Del Lama et al., 2000).

Thus, the key issues concerning A-type granitoid origin are: the role of mantle-derived material, its interaction with lower to middle continental crust, and the depth of the A-type magma production. We believe that important constraints to existing models can be obtained from study of more complete syenite–granite series and their volcanic counterparts.

Syenites in the A-type granite series are common (Whalen et al., 1987; Eby, 1990, 1992), but they are usually far exceeded in volume by granites. This may be the reason why the origin of syenite attracts less attention. Models of the A-type magma generation are based mostly on data obtained only from the study of granitic rocks. However, in some intracontinental rift zones, the proportion of syenite is significant, and it can be shown that syenite magma is

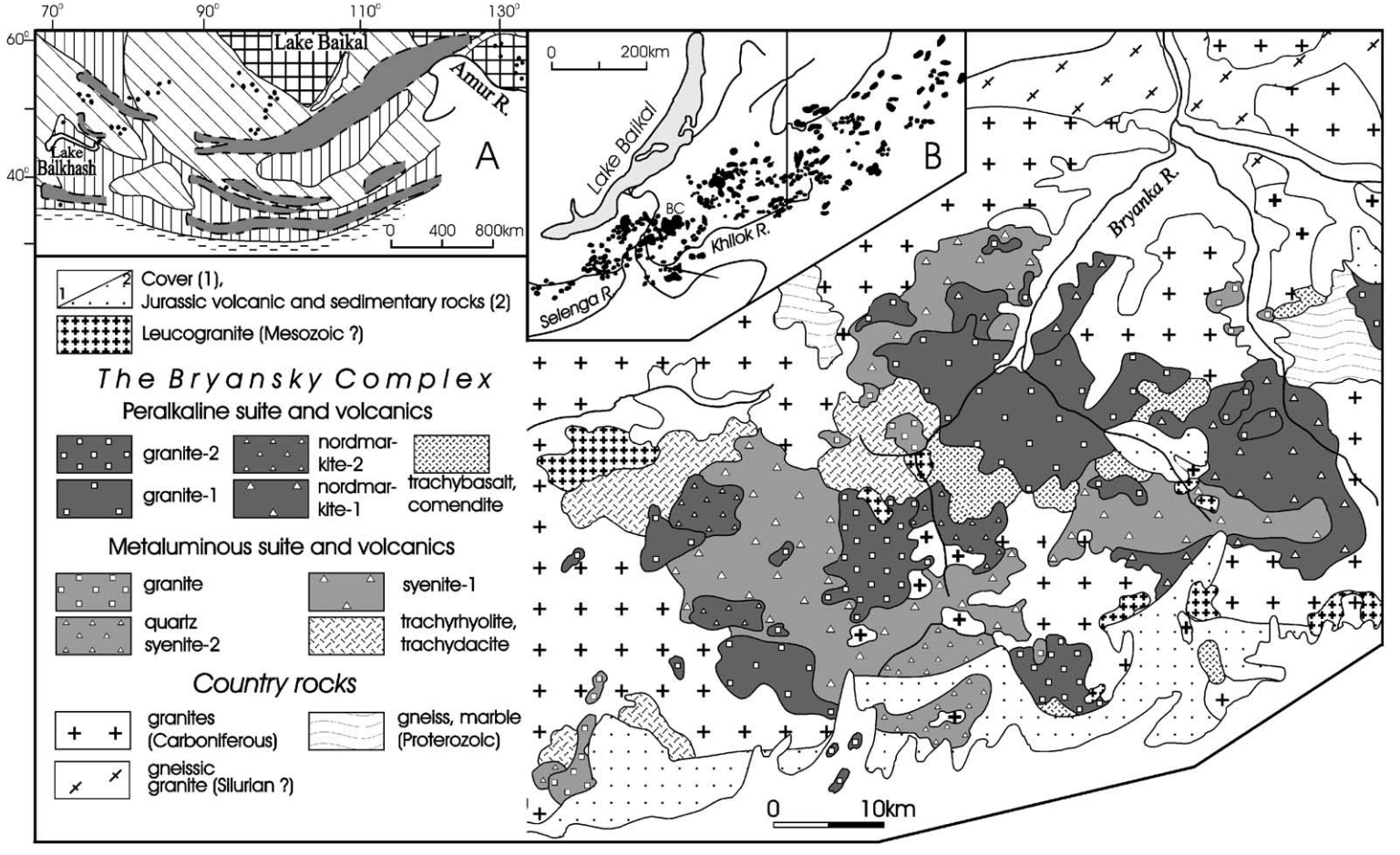

Fig. 1. Geological sketch map of the Bryansky Complex. (Inset A) Distribution of Permian–Triassic A-type granitoids in Central Asia. Shaded areas denote granitoid belts confined to the intracontinental rift zones; plutons outside these zones are shown as dots. Precambrian, Caledonian, Hercynian and Late Hercynian structures are shown by different patterns: grille, diagonal rules, vertical rules and dashes, respectively. (Inset B) Granitoid plutons from the central part of the Mongolian–Transbaikalian Belt. The Bryansky Complex is marked as BC.

parental to the whole syenite–granite series. Consequently, the origin of syenites can be considered as a key to the generation of granitoid magmas that are related to intracontinental rifting (A-1 granites of Eby, 1992).

Among the provinces in which A-type syenite–granite suites are abundant, one of the greatest is a complex network of Permian–Triassic intracontinental rift zones (~ 5000 by 2000 km), which control the occurrence of the A-type granitoid belts in Central Asia (Fig. 1, Inset A). The best studied is the Mongolian–Transbaikalian Belt (MTB) that stretches for more than 2000 km with a width of 200 to 300 km (Zanvilevich et al., 1985, 1995; Wickham et al., 1995; Litvinovsky et al., 1999). It incorporates more than 350 individual plutons (Fig. 1, Inset B). In the territory of Transbaikalia, they are referred to as three successive Permian–Triassic suites: monzonite–syenite–granite and two alkali-feldspar syenite–granite suites, metaluminous and peralkaline. All suites were formed in a similar orderly sequence, from syenite (or monzonite) through quartz syenite to granite. Each plutonic stage was preceded by the formation of alkali-rich volcanic, mostly bimodal, series (Zanvilevich et al., 1985; Yarmolyuk, 1983; Gordienko, 1987). Rocks of metaluminous and peralkaline suites commonly make up the same plutons.

In this paper, the petrogenesis of metaluminous and peralkaline syenite–granite suites, possibly the best representatives of A-type granitoids, is discussed using as an example the Bryansky Complex that is typical in composition, structure and order of formation for the MTB as a whole. To the authors' knowledge, this is the largest known peralkaline granitoid complex.

2. Geological setting and petrography

Formation of the Mongolian–Transbaikalian Granite Belt was timed to the completion of a large Paleozoic orogenic province development. The province incorporated vast territory of South Siberia (Russia) and north Mongolia, totally more than 2,000,000 km^2 (Wickham et al., 1995; Litvinovsky et al., 1999). During a period from Early Cambrian to Devonian, the geodynamic environments on this territory change from island arc through active continental margin through continental collision. Each stage was marked by formation of voluminous magmatic suites of different types. In Carboniferous, transition from compressional to tensional regime resulted in formation of the Mongolian–Transbaikalian Belt. Abundant high-K calc-alkaline granites and related volcanic series were timed to this stage. Beginning from Early Permian, the anorogenic stage commenced. Large intracontinental rift zones confined to MTB defined the magmatic activity, and abovementioned three alkali-rich granitoid series formed. Besides, it was established just recently (Litvinovsky et al., 2001; Yarmolyuk et al., 2001) that formation of peralkaline syenite–granite series occurred during two discrete stages, in the Early Permian (~ 280 Ma) and in the end of Triassic (220–210 Ma). Extensive magmatic activity controlled by the rift zones continued during the whole Mesozoic. These zones preceded the contemporary Baikal Rift formation in South Siberia.

The Bryansky Complex is confined to the central part of the MTB (Fig. 1, Inset B). It is situated in East Siberia, to the south of Lake Baikal, 200 km SE from the outfall of the Selenga River. The Complex occupies an area of about 1600 km^2. Since the southern sections of the complex are partly overlain by Early Jurassic volcanics and sediments, its real areal extent is significantly greater. The Bryansky Complex is made up of two successive syenite–granite suites, metaluminous and peralkaline. In both suites, two stages, early syenitic (or nordmarkitic) and late granitic are distinguished. The relative order of magmatic intrusions is established on the basis of crosscutting relationships. In the metaluminous suite, syenite strongly dominates over granite by 9 to 1 by volume; in the peralkaline suite, however, the proportion of syenite and granite is approximately equal. Two volcanic suites, trachydacite–trachyrhyolite and bimodal trachybasalt–comendite, preceded the emplacement of the plutonic metaluminous and peralkaline suites, respectively. A characteristic feature of the Bryansky Complex is the abundance of dikes, including peralkaline syenite, comendite, metaluminous granite-porphyry, syenite-porphyry and lamprophyre. The main succession of the Complex formation is shown in the *Legend* to the geological map (Fig. 1). Plutonic rocks of the Bryansky Complex intrude Late Paleozoic granitoids as well as Proterozoic metamor-

phic rocks. A number of small, supposedly Jurassic leucogranitic stocks intrude the magmatic rocks of the Complex.

All the main varieties of syenite and granite are leucocratic, ash-gray to pink in color, with isotropic texture. Rocks of the early phases are coarse-grained with grain size from 5 to 12 mm, while granitoids of the later phases are commonly medium-grained. Most of the coarse-grained varieties contain abundant miarolitic cavities partially filled by aggregates of quartz and mafic minerals, and occasionally with fluorite in peralkaline granites. Both syenites and granites are homogeneous. They do not contain schlierens and mafic enclaves; xenoliths of country rocks are rare and confined to the contact zone.

The absence of Ca-bearing plagioclase is characteristic of rocks from both suites. Metaluminous syenites and nordmarkites always contain quartz, and are mesoscopically similar. They may be distinguished in thin sections by the presence of Na-rich amphibole and pyroxene in nordmarkites. Metaluminous and peralkaline granites are easily distinguished by different colour (pink and ash-gray) and by mafic minerals: biotite in metaluminous granite, Na-rich amphibole and pyroxene in peralkaline ones.

Syenites from the metaluminous suite consist mainly of mesoperthitic alkali feldspar with *Ab/Or* ratio of about 1.3 (Table 1). The quartz content in syenite of the early intrusive phase (syenite-1) is, on average, 2 to 4 vol.%; in later quartz syenite (quartz syenite-2), it attains 10–12%. Mafic minerals constitute 3% to 5% of the rock volume; these are amphibole (edenite, barroisite) and biotite which is characterized by high MnO (up to 2.5 wt.%) and F (1.7–1.9 wt.%) contents (Table 2). In syenite-1, Mg-hornblende (Table 2, sample 2) and salite grains can be rarely seen. Accessories are titanite, apatite, zircon, Ti-magnetite, and allanite.

Nordmarkite, as compared with metaluminous syenite, is richer in quartz, about 5–7% in the early and up to 15–17% in the later phase. The main rock-forming mineral is also a mesoperthitic alkali feldspar with *Ab/Or* ratio = 1.5–1.7 (Table 1). Mafic minerals, riebeckite and aegirine (Tables 2 and 3), make up about 6–8% of the rock volume. In earlier nordmarkite (nordmarkite-1), riebeckite prevails while in later nordmarkite-2 both mafic minerals are present in equal amount, about 3–4 vol.%. Judging from the grain shape and relations with other minerals, riebeckite crystallized at an early stage whereas aegirine was a near-solidus mineral. In some nordmarkite, rare mafic minerals, unusual for this rock-type, appear. These are: salite with 1.2–6.6% of *Aeg* molecule (Table 3, sample 3), Na–Ca amphibole (katophorite and barroisite), and biotite. Overgrowths of riebeckite on the salite and amphibole grains suggest their

Table 1
Microprobe analyses of alkali feldspar in the representative rock types of the Bryansky Complex (wt.%)

	Syenite-1		Qtz. syenite-2	Granite	Nordmar.-1	Nordmar.-2	PA granite-1	PA granite-2
	1	2	3	4	5	6	7	8
SiO_2	66.08	65.64	65.16	66.6	66.55	67.09	65.3	66.31
Al_2O_3	19.3	20.45	18.53	18.9	18.64	17.91	18.58	17.87
FeO *	n.d.	0.24	0.44	0.2	0.49	0.35	0.47	0.63
CaO	0.41	1.31	–	0.06	0.04	–	–	–
Na_2O	6.36	8.61	6.77	7.46	7.04	7.51	6.12	6.33
K_2O	8.57	4.15	7.87	7.34	7.09	7.46	8.75	8.06
Total	100.72	100.4	98.77	100.56	99.84	100.32	99.22	99.2
An	1.9	6		0.3	0.2			
Ab	52	71.4	56.7	60.6	60	60.5	51.5	54.4
Or	46.1	22.6	43.3	39.2	39.8	39.5	48.5	45.6

(1) *Metaluminous suite*: syenite-1, qtz. syenite-2 and granite. *Peralkaline suite*: nordmar.-1, nordmar.-2, PA granite-1 and -2 (nordmarkites and peralkaline granites).
(2) FeO * = total Fe calculated as FeO.
(3) n.d. = concentration of element was not determined, hyphen = concentration of element below the detection limit.
(4) Sample 1 = alkali feldspar from syenite-1 enriched in cumulate crystals (#B400, Table 4).
(5) *An*, *Ab* and *Or* (mol%).

Table 2
Microprobe analyses of amphibole and biotite in the representative rock types of the Bryansky Complex (wt.%)

	Syenite-1		Qtz. syenite-2	Nordmarkite-1			Nordmar.-2	PA granite-1	PA granite-2	Comendite	Syenite-1	Qtz. syenite-2	Granite	Nordmar.-1	Nordmar.-2	PA granite-2
	1	2	3	4	5	6	7	8	9	10	11	12	13	14	15	16
	Amphibole										Biotite					
SiO_2	49.15	49.11	51.24	53.76	51.19	51.42	48.96	51.4	49.31	48.08	40.06	38.43	40.87	40.4	35.56	37.95
TiO_2	1.1	0.66	0.65	0.28	0.78	0.85	1.28	0.18	0.89	0.19	2.1	1.99	0.99	2.01	3.43	0.96
Al_2O_3	2.96	4.3	2.25	0.81	1.04	2.04	4.02	0.85	1.14	0.47	8.76	11.42	10.3	8.9	11.22	13.93
FeO*	19.07	13.16	10.93	15.85	26.49	16.72	17.93	23.49	25.7	30.35	17.23	18.17	13.78	17.23	24.34	16.19
MnO	1.99	1.15	4.27	1.3	1.49	1.43	1.07	1.27	2.8	0.65	1.14	1.51	2.54	0.75	0.62	0.75
MgO	10.05	14.52	14.32	12	5.1	10.96	8.82	8.07	4.56	0.23	16.13	14.57	16.87	15.46	10.12	16.62
CaO	8.1	10.32	8.07	4.9	1.15	6.68	7.35	0.79	1.76	0.26	0.1	0.18	0.03	0.09	–	–
Na_2O	3.72	1.75	3.57	6.15	7.55	5.22	5.07	7.95	7.19	13.32	0.2	0.26	0.1	0.13	0.27	–
K_2O	0.89	0.71	0.75	1.21	1.12	1.07	1.01	1.25	1.25	0.19	9.25	9.35	8.8	9.68	9.35	8.81
Total	97.03	95.68	96.05	96.26	95.9	96.39	95.51	95.23	94.6	93.74	94.97	95.88	94.28	94.64	94.91	95.21
F	0.89	0.77	1.07	1.23	0.82	n.d.	n.d.	1.44	1	n.d.	1.71	1.89	2.29	1.82	n.d.	n.d.
Cl	0.03	0.04	0.02	0.01	0.01	n.d.	n.d.	0.02	0.05	n.d.	0.04	0.06	0.04	0.01	n.d.	n.d.

Samples 2 = amphibole from syenite-1 enriched in cumulate crystals (#B400, Table 4).
(1) *Metaluminous suite*: syenite-1, qtz. syenite-2 and granite. *Peralkaline suite*: nordmar.-1, nordmar.-2, PA granite-1 and -2 (nordmarkites and peralkaline granites).
(2) FeO* = total Fe calculated as FeO.
(3) n.d. = concentration of element was not determined, hyphen = concentration of element below the detection limit.
(4) Sample 1 = alkali feldspar from syenite-1 enriched in cumulate crystals (#B400, Table 4).
(5) *An*, *Ab* and *Or* (mol%).

Table 3
Microprobe analyses of pyroxene in the representative rock types of the Bryansky Complex (wt.%)

	Syenite-1	Nordmarite-1		PA granite-1		PA granite-2	Comendite
	1	2	3	4	5	6	7
SiO_2	53.34	51.59	51.17	51.12	52.16	51.36	52.25
TiO_2	–	0.12	0.35	0.64	1.38	1.08	0.18
Al_2O_3	0.33	0.32	0.6	0.39	0.34	0.37	0.27
FeO *	9.64	25	10.35	27.49	29.3	27.69	29.36
MnO	1.15	0.82	1.46	1.08	0.33	0.97	0.78
MgO	12.33	2.59	14.89	1.15	–	0.6	0.56
CaO	22.2	8.09	20.74	5.35	0.86	3.87	1.83
Na_2O	0.78	8.62	0.3	10.01	13.25	11.39	12.52
Total	99.77	97.16	99.86	97.23	97.62	97.33	97.75
Aeg (mol%)	2.2	47.7	1.2	61.5	94.1	75.5	88.2

Sample 3 = pyroxene from nordmarkite-1 with cumulate crystals.
(1) *Metaluminous suite*: syenite-1, qtz. syenite-2 and granite. *Peralkaline suite*: nordmar.-1, nordmar.-2, PA granite-1 and -2 (nordmarkites and peralkaline granites).
(2) FeO * = total Fe calculated as FeO.
(3) n.d. = concentration of element was not determined, hyphen = concentration of element below the detection limit.
(4) Sample 1 = alkali feldspar from syenite-1 enriched in cumulate crystals (#B400, Table 4).
(5) *An*, *Ab* and *Or* (mol%).

crystallization at the magmatic stage. Accessory minerals are titanite, apatite, zircon, Fe–Ti oxides; in late nordmarkite, allanite and monazite are also distinguishable.

Granites from the metaluminous suite are micropegmatitic, graphic, and more rarely show hypidiomorphic texture. About 70% of the rock volume is made up of cryptoperthitic alkali feldspar with *Ab/Or* ~ 1.4 (Table 1). Quartz constitutes 25–30% in volume. High-magnesian biotite, similar to biotite from the metaluminous syenite (Table 2) forms single flakes. Accessories are zircon, allanite, titanite, apatite and Ti-magnetite.

Peralkaline granites also consist mainly of alkali feldspar (65–70%) and quartz (20–35%). Riebeckite and aegirine constitute 7–8% of the rock volume; in the earlier granite, they are present in equal amount, in granites of the latest phase aegirine prevails. Unlike syenite, aegirine in granite forms idiomorphic-zoned crystals (Table 3, samples 4 and 5 represent core and rim) rather than irregular interstitial grains. Fluorite is abundant among the accessory minerals that are the same as in metaluminous granite.

Comendites from the volcanic series are porphyritic and glomeroporphyritic rocks with microgranophyre or felsitic matrix. Phenocrysts are idiomorphic grains of alkali feldspar, quartz, arfvedsonite and aegirine (Tables 2 and 3). The matrix consists of the same minerals, with a predominance of aegirine over arfvedsonite.

3. Analytical methods

3.1. Mineralogy

Microprobe analyses were carried out on carbon-coated, polished thin sections using a modernized four-channel MAR-3 electron probe microanalyser at the Geological Institute, Siberian Branch of the Russian Academy of Sciences (SB RAS), Ulan-Ude, and a Cameca SX-50 at the University of Chicago. Analyses were obtained with 2–3 μm diameters beam. Operating conditions were 20 kV, 40 μA beam current, and a counting time 10 s. Generally, 11–13 elements were analysed, depending on the mineral, and oxygen obtained from stoichiometry. To determine the bulk composition of alkali feldspar, crystals were scanned. Traverses across exsolved grains were done manually, avoiding imperfections in the polish and inhomogeneously exsolved grain parts, and bulk composition was estimated by averaging the results of five to six analyses. The detection limits are 0.05–0.09 wt.% for Na_2O, MgO, Al_2O_3, and for SiO_2; 0.01–0.05 wt.% for Cl, K_2O, CaO, TiO_2, MnO, and FeO, and 0.3–0.4 wt.% for F.

Table 4
Major and trace element composition of representative samples of plutonic and volcanic rocks from the Bryansky Complex (wt.%, ppm)

Sample no.	B370	K137	B406	B400	K108	A353	B428	B425	K176	K162	K117-4	K116	K120	B627	B530	K178-1	B529-1	K109
Rock	Metaluminous syenite-1				Metaluminous Qtz. syenite-2			Metaluminous granite			Nordmarkite-1					Nordmarkite-2		
SiO_2	62.7	62.8	64.6	63.01	62.5	63.8	67.9	73.4	74.01	75.5	63.6	64.7	65.3	65.0	66.4	65.4	66.6	68.1
TiO_2	0.65	0.75	0.55	0.69	0.58	0.43	0.4	0.14	0.3	0.12	0.88	0.8	0.67	0.62	0.52	0.71	0.34	0.32
Al_2O_3	18.3	17.4	16.2	17.6	18.2	18.2	15.7	13.6	12.2	12.6	16	16.8	16.5	16.8	16	16.05	16.3	14.9
Fe_2O_3	0.87	1.1	1.61	1.6	1.34	0.72	1.36	0.7	2.2	0.59	1.36	1.77	1.53	1.64	1.7	1.57	1.22	1.62
FeO	1.9	1.9	3.49	2.43	1.76	1.88	1.41	1.05	1.17	1.19	2.29	1.94	1.94	1.01	1.64	2.24	1.14	1.39
MnO	0.09	0.09	0.1	0.09	0.15	0.14	0.12	0.05	0.01	0.04	0.17	0.12	0.12	0.12	0.12	0.19	0.08	0.05
MgO	0.3	0.6	0.36	0.61	0.33	0.18	0.24	0.1	0.11	0.08	0.6	0.54	0.4	0.28	0.31	0.38	0.23	0.21
CaO	0.98	0.92	0.43	1.47	0.67	0.76	0.35	0.12	0.1	0.14	0.3	0.51	0.46	0.75	0.43	0.6	0.52	0.38
Na_2O	6.34	5.64	5.89	6.7	6.35	6.41	5.38	4.7	3.81	4.39	6.66	6.64	6.42	6.33	6.02	6.38	5.92	5.92
K_2O	6.83	7.04	5.85	4.9	6.55	6.55	5.7	5.2	4.64	4.82	6.58	5.73	5.73	6.63	6	6.29	6.22	5.33
P_2O_5	0.08	0.12	0.08	0.15	0.07	0.06	0.05	0.03	0.01	0.01	0.12	0.15	0.1	0.04	0.02	0.05	0	0.05
LO I	1.01	1.01	0.88	0.97	1.39	0.9	1.35	1.11	1.13	0.9	1.75	0.51	1.31	0.81	0.4	0.74	1	1.35
Total	100.05	99.37	100.04	100.22	99.89	100.03	99.96	100.2	99.69	100.38	100.31	100.21	100.48	100.03	99.56	100.6	99.57	99.62
AI	0.97	0.97	0.99	0.93	0.96	0.97	0.96	0.98	0.93	0.99	1.13	1.02	1.02	1.05	1.02	1.08	1.01	1.04
ASI	0.93	0.94	0.96	0.93	0.97	0.96	1.0	1.0	1.06	0.99	0.86	0.93	0.94	0.89	0.93	0.87	0.94	0.92
Rb	97	100	150	70	120	68	110	170	150	170	82	67	81	130	160	110	170	240
Ba	880	780	390	4400	106	260	840	250	65	50	100	540	250	80	110	200	170	30
Sr	190	42	52	450	27	49	84	47	15	6	14	65	28	34	35	29	45	5
Zr	340	260	610	270	150	72	360	190	290	250	250	140	250	930	700	230	490	780
Nb	16	21	27	16	11	7	16	20	32	26	24	13	21	38	32	33	24	50
Y	32	76	53	32	19	10	36	19	29	46	35	23	29	64	49	39	30	56
Th	5	9	28	7	5	2	13	23	28	21	4.3	5.1	5.5	n.d.	n.d.	11	n.d.	16
Hf	10	5.7	15	15	4.2	1.4	11	6.2	n.d.	n.d.	4.2	4	6.3	n.d.	n.d.	7.2	n.d.	16
Ta	1.2	2.4	1.5	1.5	0.28	0.21	1.1	1.3	n.d.	n.d.	0.7	0.8	0.9	n.d.	n.d.	1.4	n.d.	n.d.
La	65	88	120	51	41	28	42	32	n.d.	n.d.	50	56	79	n.d.	n.d.	120	n.d.	n.d.
Ce	140	200	260	110	74	52	97	61	n.d.	n.d.	110	110	140	n.d.	n.d.	240	n.d.	n.d.
Nd	69	89	100	54	30	24	40	15	n.d.	n.d.	42	52	48	n.d.	n.d.	81	n.d.	n.d.
Sm	11	20	13	7.5	4.5	4.4	5.7	1.9	n.d.	n.d.	7.8	7.2	6.3	n.d.	n.d.	12	n.d.	n.d.
Eu	1.8	2.9	1.4	3.2	0.59	0.65	1.01	0.21	n.d.	n.d.	1.1	1.3	1.1	n.d.	n.d.	1.2	n.d.	n.d.
Tb	1.3	2.9	1.6	1	0.53	0.39	0.79	0.26	n.d.	n.d.	0.84	0.82	0.77	n.d.	n.d.	1.5	n.d.	n.d.
Yb	2.8	5.1	4.4	2.8	1.3	1.1	3.1	2	n.d.	n.d.	2.3	1.7	2.8	n.d.	n.d.	3.6	n.d.	n.d.
Lu	0.41	0.68	0.58	0.38	0.21	0.17	0.47	0.32	n.d.	n.d.	0.34	0.23	0.45	n.d.	n.d.	0.51	n.d.	n.d.
Eu/Eu*	0.53	0.45	0.34	1.34	0.42	0.5	0.55	0.35			0.46	0.59	0.56			0.32		

Sample No	K158	B432-1	B378	B405	B434	B371	B625	B426	B388	B435	B389	A447-4	B382-2	K116-2	K168	B386
Rock	Nordmarkite-2		Peralkaline granite-1					Peralkaline granite-2				Comendite				Tr-andes.
SiO_2	68.1	68.80	69.8	70.8	72.6	74	75.02	69.6	72.6	73.5	74.4	71.8	72.5	74.2	74.8	61.9
TiO_2	0.51	0.60	0.4	0.46	0.26	0.21	0.32	0.4	0.3	0.22	0.21	0.51	0.42	0.24	0.41	0.6
Al_2O_3	14.8	14.30	13.6	12.8	12.4	12	10.65	14.4	12	12.05	10.6	10.9	11	12.2	10.9	16.5
Fe_2O_3	1.5	1.46	1.5	1.85	0.85	0.87	2.15	1.54	2.4	1.05	3	3	4.45	1.9	0.15	1.84
FeO	1.18	2.11	2.09	1.61	1.85	1.48	1.35	1.32	1.59	1.76	1.59	1.9	1.17	1.61	1.63	3.86
MnO	0.11	0.12	0.15	0.14	0.1	0.1	0.17	0.16	0.11	0.04	0.19	0.2	0.21	0.12	0.03	0.09
MgO	0.33	0.29	0.41	0.24	0.14	0.21	0.13	0.27	0.23	0.14	0.21	0.13	0.23	0.16	0.2	1.72
CaO	0.02	0.26	0.32	0.26	0.05	0.14	0.03	0.02	0.15	0.04	0.5	0.02	0.25	0.04	0.02	2.8
Na_2O	5.94	5.26	5.1	5.19	4.66	4.4	4.51	5.78	4.76	4.39	4.21	4.77	4.41	4.84	2.64	4.59
K_2O	6.19	5.61	5.56	5.58	5.33	4.66	4.73	5.4	4.74	4.94	4.6	4.57	4.5	3.88	6.88	4.14
P_2O_5	0.04	0.06	0.04	0.04	0.03	0.02	0.01	0.03	0.01	0.02	0	0.02	0.01	0.05	0.03	0.18
LO I	1.4	1.14	1.33	0.77	1.4	1.36	0.34	1.3	0.97	1.59	0.84	1.71	0.83	0.68	2.01	1.8
Total	100.12	100.01	100.3	99.74	99.67	99.45	99.41	100.22	99.86	99.74	100.35	99.54	99.99	99.92	99.7	100.02
AI	1.11	1.06	1.06	1.14	1.08	1.02	1.18	1.07	1.08	1.04	1.12	1.17	1.1	1.0	1.08	
ASI	0.9	0.94	0.91	0.85	0.92	0.96	0.85	0.94	0.91	0.95	0.83	0.85	0.87	1.0	0.92	
Rb	190	150	260	215	210	250	290	120	190	200	200	260	270	170	360	100
Ba	32	310	150	98	125	66	40	63	47	160	55	10	24	66	100	1500
Sr	5	61	19	13	32	12	9	7	5	40	4	38	13	12	20	660
Zr	710	710	850	700	480	560	1070	450	470	380	980	2200	1550	2000	1950	310
Nb	33	36	63	46	26	47	50	22	35	23	27	120	84	97	98	15
Y	60	83	110	81	35	77	66	52	80	35	53	170	130	190	150	27
Th	19	33	43	27	32	38	36	18	11	25	26	67	51	60	46	15
Hf	22	17.0	14	21	13	21	32	11	18	16	23	53	36	50	42	8.3
Ta	2.6	2.80	4.9	3.5	n.d.	4.2	3.4	1.7	2.6	2.3	n.d.	7.4	5.2	n.d.	n.d.	0.97
La	140	79	98	96	n.d.	66	107.5	40	75	53	n.d.	150	90	n.d.	n.d.	50
Ce	310	240	220	200	n.d.	170	151.6	110	160	110	n.d.	340	270	n.d.	n.d.	92
Nd	120	90.0	84	82	n.d.	67	59.3	31	60	35	n.d.	110	67	n.d.	n.d.	35
Sm	14	16.0	13	12	n.d.	12	9.4	4.9	10	5	n.d.	19	14	n.d.	n.d.	6.6
Eu	1.1	1.50	1.1	1.1	n.d.	0.77	0.67	0.52	1.01	0.34	n.d.	1.6	1.1	n.d.	n.d.	1.2
Tb	1.9	2.60	2.2	2.2	n.d.	2.3	2.76	0.82	2	0.87	n.d.	4.3	3.1	n.d.	n.d.	0.8
Yb	5.1	6.10	8.5	8.4	n.d.	7.9	6.85	3.5	8.1	4	n.d.	16	12	n.d.	n.d.	2.5
Lu	0.85	0.78	1.3	1.2	n.d.	1.1	1.1	0.55	1.1	0.62	n.d.	2.5	2	n.d.	n.d.	0.4
Eu/Eu *	0.25	0.28	0.25	0.27		0.18	0.21	0.32	0.29	0.2		0.23	0.22			0.58

AI=$(Na_2O + K_2O)/Al_2O_3$ (mol%); *ASI* = $Al_2O_3/(CaO + Na_2O + K_2O)$ (mol%); tr-andes. = trachyandesite.

3.2. Geochemistry

All analyses were done using a combination of wet chemical method, AAS and titration (major elements), and X-ray fluorescence (Rb, Sr, Ba, Y, Zr, Nb, and Th) at the Geological Institute of SB RAS, Ulan-Ude. Rare earth elements were determined mainly by instrumental neutron activation at the Analytical Center of Geological Institute RAS (Moscow), some samples were analysed by the ICP-MS method in the Rennes University. Analyses are considered accurate to within 2–5% for major elements, and better than 10–15% for trace elements. The accuracy for all the REE (except Lu) is 1–5%, for Lu—9–10%.

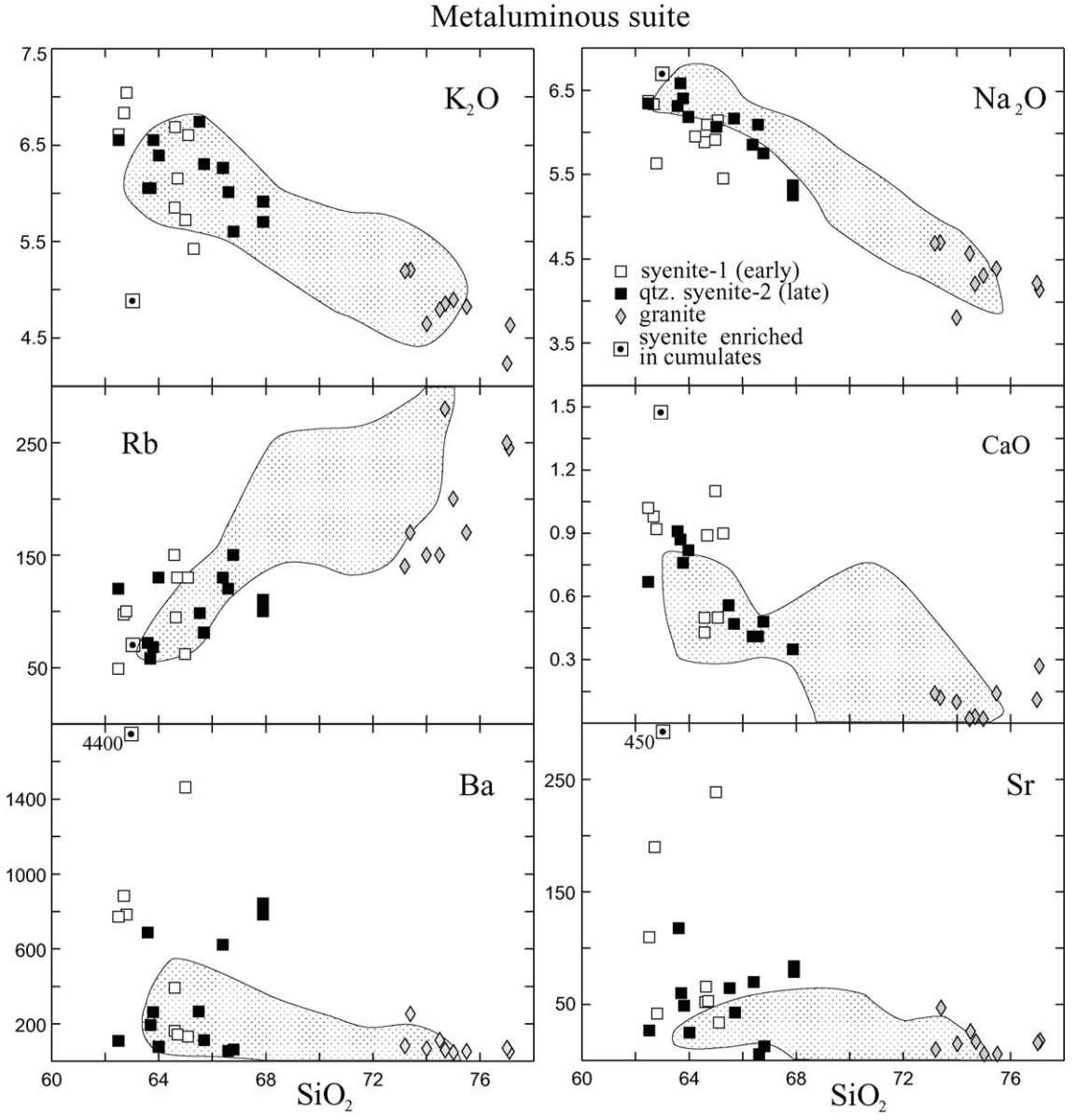

Fig. 2. Silica variation diagrams for selected major and trace elements for the metaluminous suite. The shaded fields are the compositions of peralkaline granitoids.

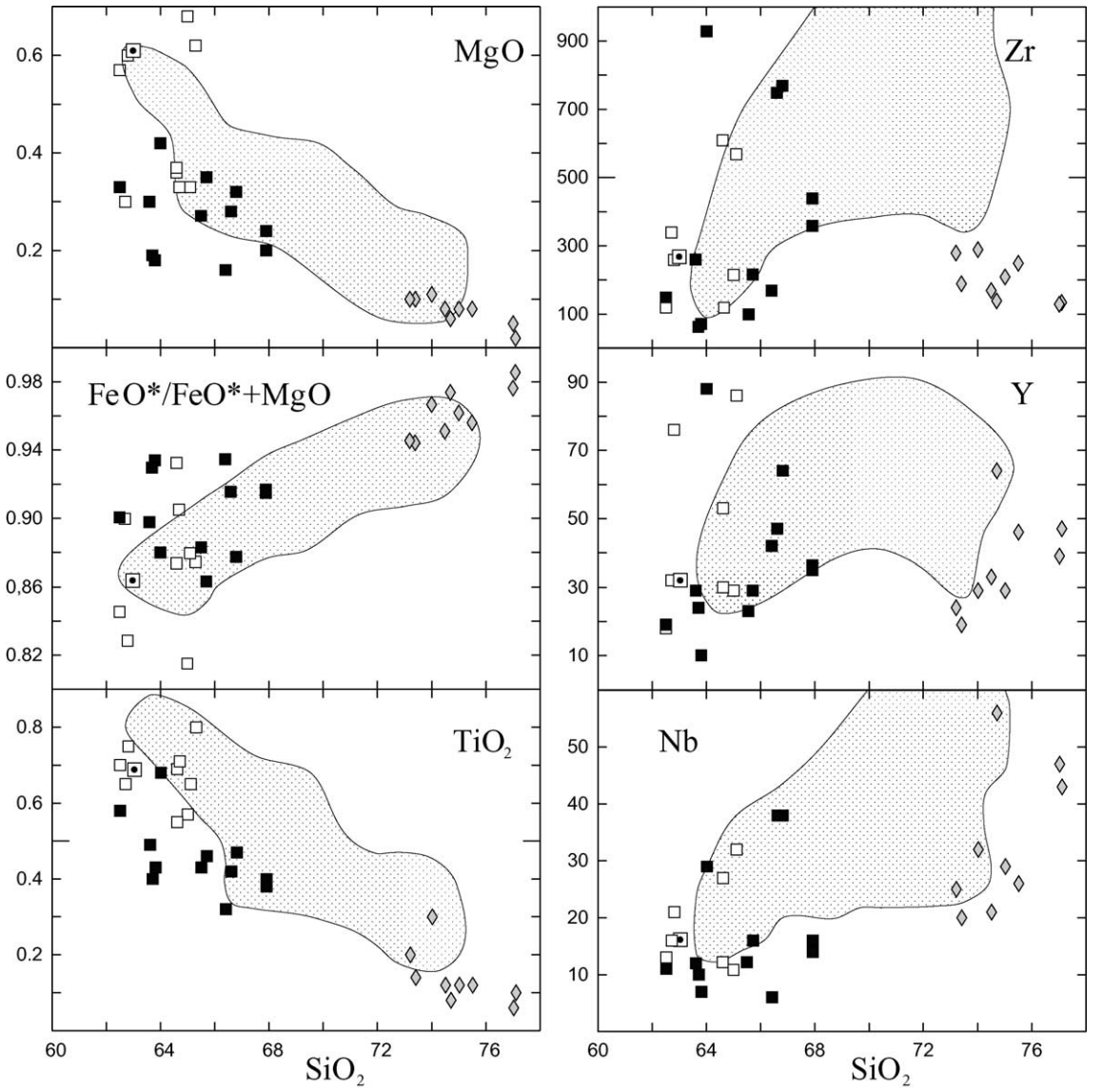

Fig. 2 (*continued*).

Normalized trace element concentrations were calculated with respect to chondrite and primitive mantle (Sun and McDonough, 1989).

3.3. Rb–Sr and Sm–Nd isotopes

Rb–Sr isotope compositions were determined for 33 whole-rock samples and 6 essentially mafic and felsic fractions of peralkaline granite composed mainly of Na-rich amphibole and pyroxene and of perthitic feldspar with quartz intergrowth, respectively. Of these, 10 whole-rock samples were further analyzed for Sm–Nd isotope compositions. The isotope ratios were measured at the Universite de Rennes, France (Rb–Sr and Sm–Nd) and at the Geological Institute of SB RAS, Ulan-Ude (Rb–Sr). Contents of Rb, Sr, Sm and Nd (Tables 5 and 6) were measured by isotope dilution mass spectrometry. The analytical techniques

at Rennes can be found in Jahn et al. (1996). Mass analyses were performed using a 7-collector Finnigan MAT-262 mass spectrometer in static mode for Sr and dynamic mode for Nd. $^{87}Sr/^{86}Sr$ ratios were normalized against the value of $^{87}Sr/^{86}Sr = 0.1194$. Long-term replicate analyses (>150) on NBS-987 Sr standard yielded $^{87}Sr/^{86}Sr = 0.710259 \pm 5$ (2σ). $^{143}Nd/^{144}Nd$ ratios were normalized against the value of $^{146}Nd/^{144}Nd = 0.7219$. Long-term replicate analyses (>150) on an in-house (Rennes) Ames Nd standard gave $^{143}Nd/^{144}Nd = 0.511966 \pm 5$ (2σ), which is equivalent to the La Jolla Nd standard of 0.511860. At the Geological Institute, the Rb and Sr isotope ratios were measured on a MI-1201 T mass spectrometer; the mean $^{87}Sr/^{86}Sr$ ratios for the VNIIM standard was 0.707988.

The notations of ε_{Nd} and $f_{Sm/Nd}$ are defined as:

$$\varepsilon_{Nd} = [(^{143}Nd/^{144}Nd)_s/(^{143}Nd/^{144}Nd)_{CHUR} - 1] \times 10,000$$

$$f_{Sm/Nd} = [(^{147}Sm/^{144}Nd)_s/(^{147}Sm/^{144}Nd)_{CHUR}] - 1$$

where s = sample, and $(^{143}Nd/^{144}Nd)_{CHUR} = 0.512638$, and $(^{147}Sm/^{144}Nd)_{CHUR} = 0.1967$. The decay constants ($\lambda$) used in age calculations are 0.0142 Ga^{-1} for ^{87}Rb and 0.00654 Ga^{-1} for ^{147}Sm. Depleted mantle Sm–Nd model ages were calculated assuming a single-stage (T_{DM}) and a two-stage (T_{DM}-2) evolution from $\varepsilon_{Nd}(T) = 0$ at 4.56 Ga to +10 at the present time.

Isochron ages were calculated using the regression program of ISOPLOT (Ludwig, 1999). Input errors are 2% for $^{87}Rb/^{86}Sr$, 0.005% for $^{87}Sr/^{86}Sr$. Unless specified, the errors quoted in age computation represent ± 2 standard-deviation (2σ).

3.4. U–Pb isotope analysis

Zircons from two representative samples were analyzed by the U–Pb method at the Natural Environment Research Council Isotope Geosciences Laboratory (NIGL), UK. These samples are B626-1 (metaluminous syenite, five zircon crystals) and B627 (nordmarkite, four crystals). Heavy minerals were obtained from 1500 to 2000 g of each sample by using standard crushing techniques at the Geological Institute, Ulan-Ude. Mineral separates were further refined using a Franz magnetic separator, and handpicked under ethanol, and only clear, crack-free grains were selected for analysis. To remove metamict grains and the radiation-damaged lattice, abrasion was performed using pyrite at air pressures between 1.0 and 5.0 PSI, until about 20% of the grain size was removed. Before dissolution zircons were washed in distilled 4 N HNO_3 followed by water. Samples were spiked with a $^{205}Pb/^{235}U$ tracer before digestion. Zircons were digested in 29N HF with a trace of HNO_3. Chemical separations followed those of Krogh (1973) with modifications (Corfu and Noble, 1992). Data were obtained on a VG 354 mass spectrometer with an ion-counting Daly detector (following Noble et al., 1993). Procedural blanks were <10 pg Pb and <1 pg U. All the data were reduced assuming a maximum of a 10-pg procedural blank, the remainder being allocated to common Pb in the minerals analysed (the ages determined this way are insignificantly different from those calculated if all the common Pb is assumed to be due to procedural contamination). Ages were calculated by using the decay constants of Jaffey et al. (1971). Errors quoted for the isotope ratios are 2σ and were calculated after the method of Ludwig (1980). Raw mass spectrometer data were reduced using the Pbdat and Isoplot programs of Ludwig (1991) and Ludwig and Titterington (1994). Initial common Pb in the mineral fractions was estimated using the method of Stacy and Kramer (1975).

3.5. Melt inclusions in rock-forming minerals

Microinclusions of crystallized melt were investigated using a heating stage with a silicon-carbide heating element. Temperatures were measured with a Pt/Pt-Rh thermocouple calibrated against known melting points of a number of chemically pure materials (salts, Ag, Au). Precision of measurement is better than ± 10 °C within the temperature interval 700–1000 °C. The homogenized melt inclusions (artificial glass) were analyzed on Camebax-micro instrument in UIGGM, Novosibirsk. For electron microprobe analyses, beam conditions were 20 kV, 20 nA beam current, using a spot size of 6–7 μm across.

The experimental procedure involves step-by-step heating of the sample (a piece of double polished

plate) until complete homogenization of melt inclusions is attained. It incorporates a series of consecutive continuous heating to a given, each time higher, temperature, with subsequent quenching (cooling rate ~ 70–80 °C s^{-1}), and optical study of the sample at high magnification (up to 1200 ×) after each experiment. To obtain equilibrium conditions for smaller melt inclusions (1–3 μm in diameter), the duration of heating was between 2.5 and 3 h in each experiment. Crystallized melt inclusions represent polycrystalline aggregates in which gas and fluid phases can be commonly distinguished only after heating. A narrow interval of homogenization temperature (T_h) in groups of inclusions within one crystal or grain, as well as systematic decrease of T_h from the core to margins of zoned crystals, suggests that these melt inclusions represent completely crystallized melt captured by the growing crystal. To obtain reliable results, groups of several (up to 50–100 in quartz) of the smallest inclusions, 1–3 μm in diameter, were studied. For determination of the melt composition, the largest inclusions (6–10 μm) were homogenized, and then the glass was subjected to microprobe analysis. Three to four hour heating of these melt inclusions at a temperature 50–80 °C higher than the T_h of small, 1–3 μm inclusions was necessary to obtain homogeneous glass.

4. Geochemistry

Major and trace element compositions were determined for about 100 samples; of these, 26 samples were analyzed for rare earth elements (REE). Data for 34 representative samples are reported in Table 4, up to 95 samples are plotted in the various geochemical diagrams (Figs. 2–5).

A common feature of the rocks from both suites is high content of total alkalis, 12–13 wt.% in syenites and about 10 wt.% in granites. Significant overlap of their chemical composition (Figs. 2–5) points to similarity of the two syenite–granite suites. At the same time, the peralkaline syenites, compared to the metaluminous, tend to contain slightly more Na_2O and less CaO, Sr and Ba; in the peralkaline granites the Zr and Y concentrations are noticeably higher than in metaluminous (Fig. 2). The agpaitic index (AI) values in the peralkaline suite is always >1, in the metaluminous granitoids the AI value ranges within 0.8–1.0 (Table 4). The aluminium saturation index (ASI) values are similar in the both suites; they are close to unit (0.92–0.99) and only some leucogranites are weakly peraluminous (Table 4).

The trends of compositional evolution from syenite to granite are not similar in the two suits. In *metaluminous suite*, going from syenite-1 to quartz syenite-2, the contents of TiO_2, MgO, CaO, Na_2O tends to decrease, concurrently with SiO_2 increase, while Zr, Y and Nb concentrations do not change (Fig. 2). The REE abundance patterns indicate a decrease of REE content from the earlier to late syenites (Fig. 3A). The Eu anomaly (Eu/Eu*) increases only slightly, from an average of 0.44 in the first phase syenite to 0.49 in the second (Table 4). Of the granites, low CaO, MgO, Sr and Ba contents are characteristic. However, Rb concentration in the granite is markedly higher than in syenite, even though the alkali concentrations de-

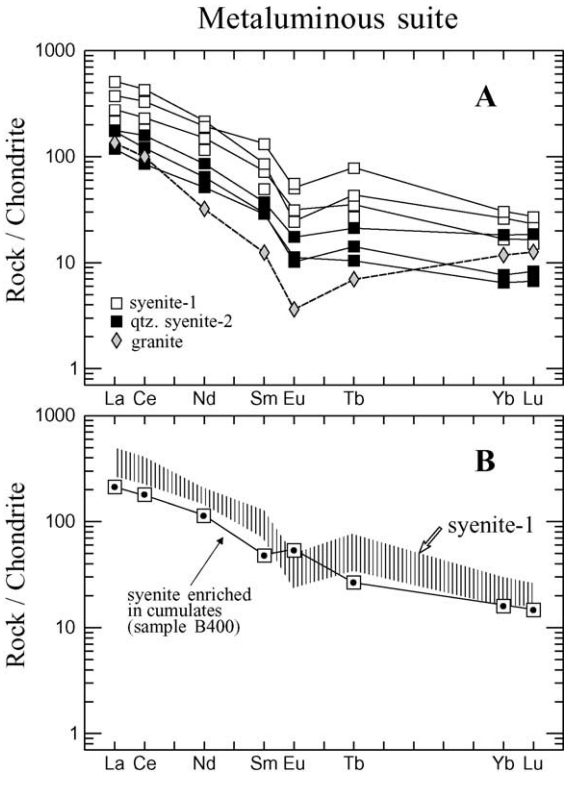

Fig. 3. Chondrite-normalized REE patterns of syenites and granites from the metaluminous suite. Chondrite values are from Sun and McDonough (1989).

crease. The Y, Nb and Zr concentrations are similar to the syenite (Table 4, Figs. 2 and 3).

Peralkaline suite is compositionally continuous (Fig. 4). The trend is exhibited by the systematic changes for some major and trace elements (MgO, alkalis, Rb, FeO*/FeO* + MgO). The general increase of REE and HFSE from early to late nordmarkite is followed by a decrease of REE in granites. The content of Zr, Y, Nb and Hf does not change noticeably (Figs. 4 and 5).

It is significant that metaluminous syenites, in spite of their leucocratic appearance and visible homoge-

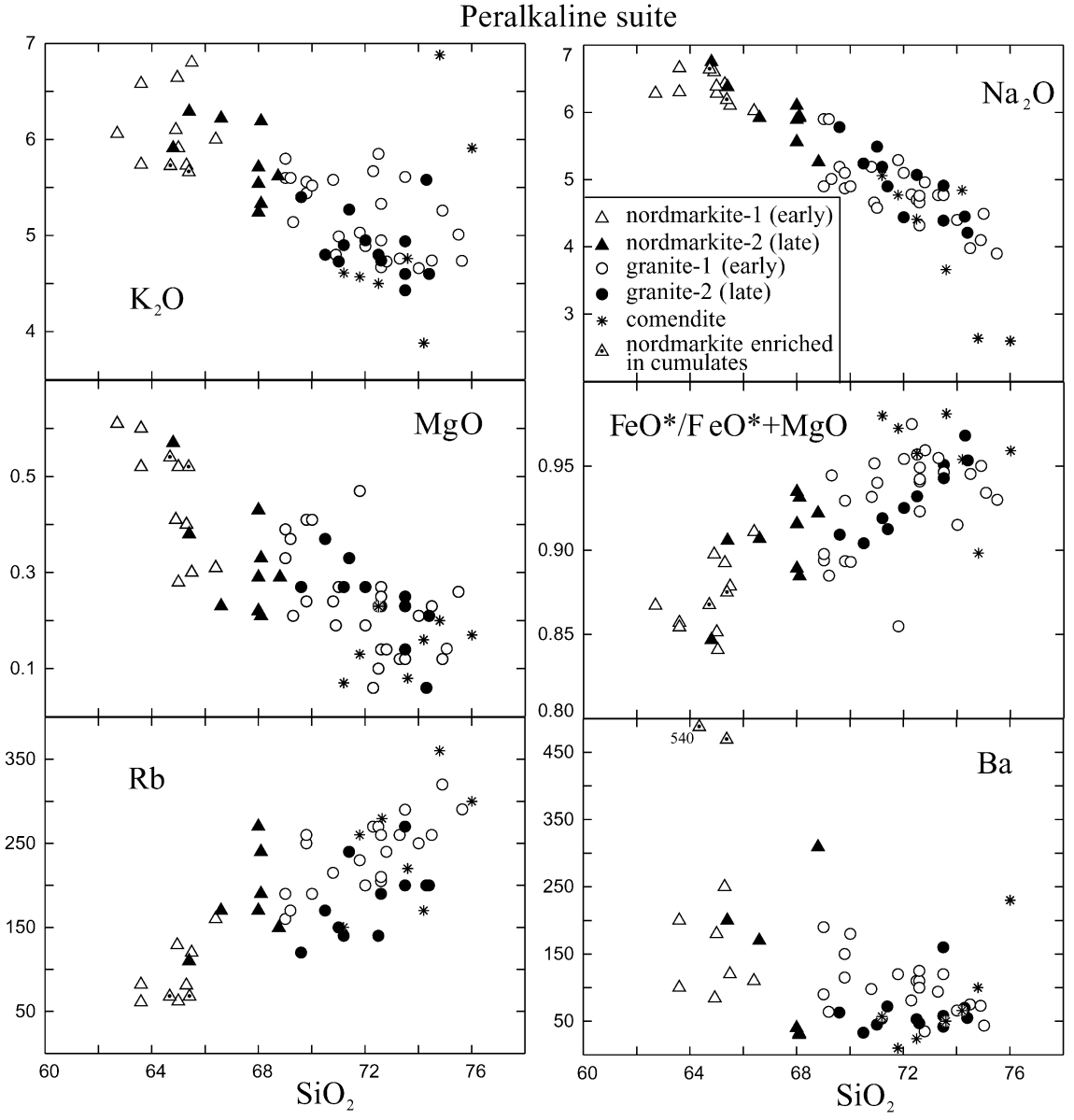

Fig. 4. Silica variation diagrams for selected major and trace elements for the peralkaline suite. The regression lines calculated for selected HFSE in the early and late nordmarkites are shown (see text).

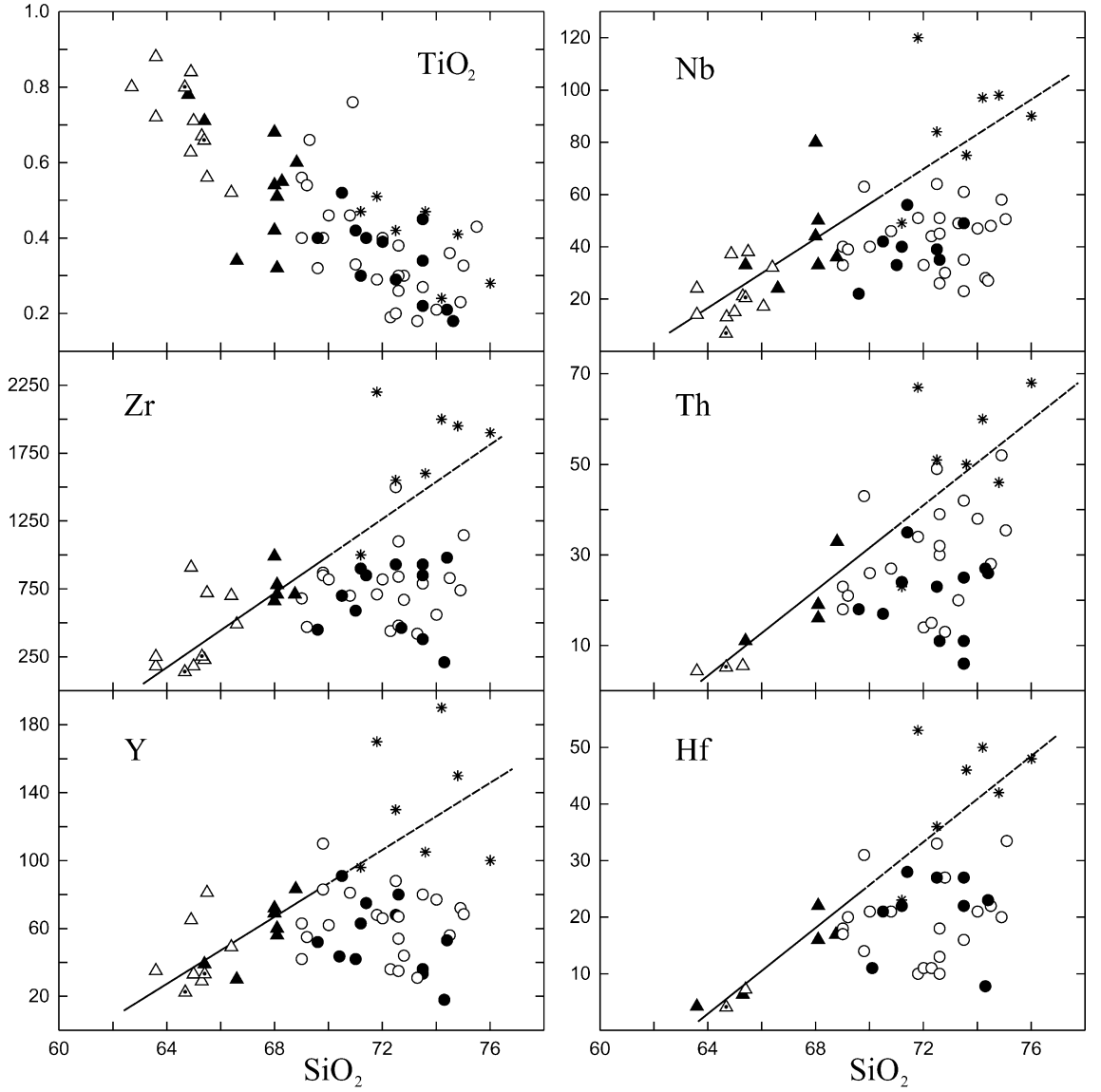

Fig. 4 (*continued*).

neity, show an heterogeneous chemical composition and are characterized by a broad range of major and some trace element contents at the same SiO_2 contents (Fig. 2). The most anomalous data in this respect is obtained in sample B400 (Table 4; Figs. 2 and 3B). Sample B400 has a positive Eu anomaly (Eu/Eu* = 1.34), elevated contents of CaO, MgO, Sr and Ba and comparatively low abundances of K, Rb, Zr, Nb and REE. This suggests enrichment in a cumulus phase, particularly feldspar. The assumption is corroborated by the presence in sample B400 of alkali feldspar grains with unusually high contents of CaO, up to 1.3 wt.% (Table 1, sample 2) and of Mg-hornblende (Table 2, sample 2), whereas edenite and barroisite are typical of metaluminous syenite of the Bryansky Complex. Consequently, the chemical heterogeneity of the metaluminous syenites probably reflects the presence of cumulus crystals, mainly

alkali-feldspar, in these rocks. The nordmarkites also include varieties abnormally enriched in Ba and Sr (Fig. 4; Table 4, sample K 116). Judging from the presence of salite and katophorite grains rimmed by aegirine and riebeckite, we suggest that some nordmarkites contain cumulus phases as well. However, REE abundances in these samples are the same as in the nordmarkite with low Ba and Sr concentration (Table 4, Fig. 5A). This suggests that the proportion of cumulus crystals is small causing only Ba and lesser Sr enrichment.

The chemical composition of the *comendites* is closely similar to that of the peralkaline granites (Fig. 4). The comendites show a greater abundance of HFSE that are mainly concentrated in accessory minerals (Zr, Y, Nb, Hf, Th, REE), whereas the Eu/Eu* value for the granites and comendite is similar, 0.23 (Table 4). Note that in plots of SiO_2 vs. Zr, Nb, Y, Th, and Hf (Fig. 4), the comendite data points are arranged

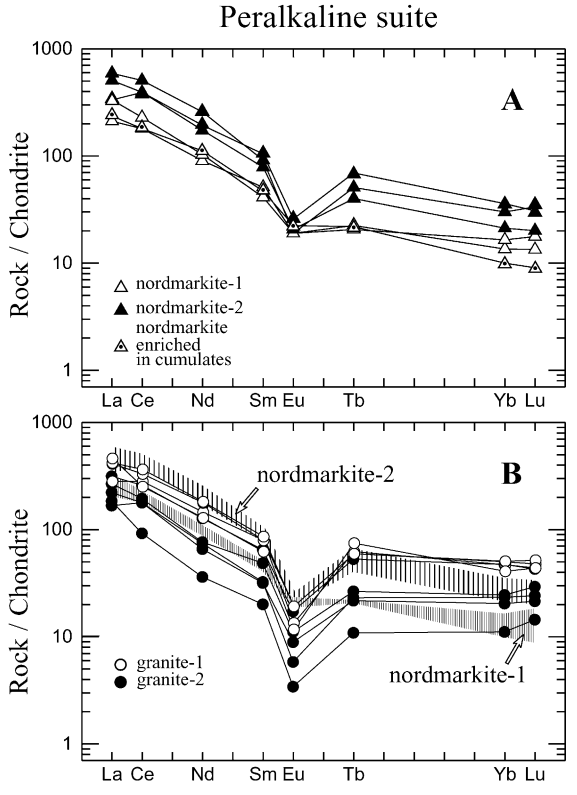

Fig. 5. Chondrite-normalized REE patterns of nordmarkite and granite from the peralkaline suite. Chondrite values are from Sun and McDonough (1989).

along the regression lines calculated for nordmarkite of early and late intrusive phases while the field of granite compositions is located far below these lines.

5. Isotope data

The Rb–Sr isotope data are given in Tables 5 and 6 and graphically represented in Fig. 6. We assume the granitic and syenitic samples to have a cogenetic relationship and a similar initial Sr isotopic ratio. Because of the very high Rb/Sr and hence very radiogenic Sr isotope ratios for these rocks, a small variation in initial $^{87}Sr/^{86}Sr$ between individual rocks would not significantly affect isochron age calculation. In the present case, the scatter of data points seems quite large, so the age obtained is not strictly an isochron age as evidenced by the large MSWD value of 12 for the peralkaline suite (Fig. 6A) and 9 for the alkali feldspar suite (Fig. 6B). The age estimation proved to be similar for both suites, 280 ± 6 Ma in peralkaline and 280 ± 14 Ma in the metaluminous suite (Fig. 6A and B).

Isochrons were also calculated for the volcanic comendite and trachyandesite as well as for the dike rocks of trachyrhyodacite and comendite composition (Fig. 6C). The volcanic rocks exhibit the age similar to granitoids, 284 ± 4 Ma, while dikes are younger, 268 ± 8 Ma. Initial strontium ratios are very similar in peralkaline and metaluminous suites, 0.7053 ± 0.0008 and 0.7050 ± 0.0010; for the volcanic suite $(^{87}Sr/^{86}Sr)_T$ is 0.7062 ± 0.0002 while for the dikes it is much lower, 0.7038 ± 0.0011.

Analytical results for five zircon aliquots from the metaluminous syenite and four zircon aliquots from the peralkaline syenite are plotted in Fig. 7. Most data points are slightly discordant with one aliquot for each sample having experienced significant Pb-loss. Therefore, the $^{206}Pb/^{238}U$ ages range from 275 to 280 Ma (metaluminous syenite) and from 270 to 280 Ma (peralkaline syenite). The $^{207}Pb/^{235}U$ ages differ only slightly from the $^{206}Pb/^{238}U$ ages for every aliquot and vary from 276 to 280 Ma (metaluminous syenite) and within the range 271–281 Ma (peralkaline syenite). We interpret the discordance to indicate recent Pb-loss as the data define chords with lower intercepts of 0. Consequently, we consider that the best estimate for the age of intrusion of both syenite types comes from

Table 5
Rb–Sr data on plutonic rocks and dikes from the Bryansky Complex

ID no.	Sample no.	Rock type	Rb (ppm)	Sr (ppm)	$^{87}Rb/^{86}Sr$	$^{87}Sr/^{86}Sr$	$\pm 2\sigma$
Peralkaline suite							
1	K116	nordmarkite	93.47	63.86	4.238	0.71778	0.00014
2	B400-1	nordmarkite	84.16	15.15	16.17	0.77034	0.00013
3	K116-1?	nordmarkite	106.50	8.55	36.58	0.85779	0.00013
4	B428	nordmarkite	118.10	87.99	3.889	0.7213	0.00005
5	K117-4	nordmarkite	55.26	14.89	10.86	0.7498	0.00016
6	B406-1	nordmarkite	109.40	21.12	15.08	0.76823	0.00012
7	B406-2	nordmarkite	120.00	15.4	22.72	0.7934	0.00015
8	B432-1	nordmarkite	171.2	63.83	7.777	0.73425	0.00006
9	B381	granite	297.7	17.26	50.59	0.92029	0.0001
10	B378	granite	283.6	38.72	21.35	0.7882	0.00011
11	B380-1	granite	308.7	22.32	40.61	0.86311	0.00011
12	B371	granite	285.9	17.38	48.45	0.89179	0.00011
13	$B371^{S}$	granite	437.3	13.8	95.01	1.07786	0.00014
14	$B371^{M}$	granite	172.9	81.4	6.16	0.72913	0.00008
15	B372	granite	286	19.85	41.6	0.86851	0.00011
16	$B372^{S}$	granite	386.80	14.06	82.25	1.04614	0.00011
17	$B372^{M}$	granite	250.2	81.34	8.928	0.74038	0.00011
18	B373	granite	249.9	33.84	21.01	0.78635	0.00008
19	$B373^{S}$	granite	328.5	17.23	56.34	0.92739	0.00014
20	$B373^{M}$	granite	94.48	77	3.554	0.71891	0.00009
Metaluminous suite							
21	B370	syenite	104.1	191.3	1.58	0.71179	0.00009
22	B400	syenite	74.22	457.8	0.47	0.70744	0.00007
23	K113	granite	273.3	18.08	44.53	0.89117	0.00009
Dikes							
24	102	comendite	304.7	6.52	141.1	1.24198	0.00052
25	104	trachyrhyodacite	129.8	20.08	18.52	0.77539	0.00093
26	105	trachyrhyodacite	125.6	30.97	11.59	0.74882	0.00023
27	106	trachyrhyodacite	131.8	11.77	32.21	0.8246	0.00076

(1) The isotope ratios were measured at the Geological Institute of the Siberian Branch, RAS (Ulan-Ude).
(2) Samples marked with superscripts "S" and "M" are felsic (mainly Afs) and mafic (Amph + Cpx) fractions, respectively.
(3) NBS 987 Sr standard = 0.710250; VNIIM Sr standard = 0.70801.
(4) Initial $^{87}Sr/^{86}Sr$ ratios calculated with $T_1 = 280$ Ma for plutonic rocks and $T_2 = 268$ Ma for dikes.
(5) Errors in $^{87}Sr/^{86}Sr$ are 2σ (in-run precision). $(^{87}Sr/^{86}Sr)_T$ is 2σ propagated to include individual within-run error, reproducibility of standard analyses, and uncertainty in Rb/Sr ratios.

a weighted mean of the $^{207}Pb/^{206}Pb$ ages which are 283 ± 5 Ma for the metaluminous syenite and 279 ± 2 Ma for the peralkaline syenite, respectively. Both results are within the error and therefore indicate that the intrusion of both types of magmas occurred at ~ 280 Ma. This age estimate is actually the same as that obtained by Rb–Sr isotope dating.

The $\varepsilon_{Nd}(T)$ values are quite uniform (Table 6). In the metaluminous suite, they range from -1.9 to -3.0; for nordmarkite, $\varepsilon_{Nd}(T) = -2.4$, while for the peralkaline granite it is -2.1. For comendite from the volcanic suite two values are obtained, -2.2 and -2.7. Thus, all $\varepsilon_{Nd}(T)$ values almost completely overlap each other. Although in trachyandesite the $\varepsilon_{Nd}(T)$ value is slightly higher, -3.5, it also remains within the error of the peralkaline and metaluminous suites.

6. Inclusions of melt in rock-forming minerals

Crystallized melt inclusions have been studied in quartz and in a few pyroxene grains. The study

Table 6
Rb–Sr and Sm–Nd data on plutonic and volcanic rocks from the Bryansky Complex and the Tsagan–Khurtei Range

ID no.	Sample no.	Rock type	Rb (ppm)	Sr (ppm)	$^{87}Rb/^{86}Sr$	$^{87}Sr/^{86}Sr$	$\pm 2\sigma$	$(^{87}Sr/^{86}Sr)_T$	Sm (ppm)	Nd (ppm)	$^{147}Sm/^{144}Nd$	$^{143}Nd/^{144}Nd$	$\pm 2\sigma$	$\varepsilon_{Nd}(0)$	f(Sm/Nd)	$\varepsilon_{Nd}(T)$	T_{DM}
Bryansky Complex (280 Ma)																	
1	B627	nordmarkite-1	141.5	45.49	9.01	0.739562	0.000008	0.70315	18.74	113.46	0.0999	0.512336	4	−5.9	−0.49	−2.4	1090
2	B388	PA granite-2	204.1	7.09	85.8	1.037942	0.00001	0.70342	10.92	56.44	0.117	0.512383	4	−5	−0.41	−2.1	1208
3	B626	syenite-1	105.4	55.77	5.46	0.726765	0.000007	0.7047	16.37	97.7	0.1013	0.512312	4	−6.4	−0.49	−3.0	1136
4	B626-1	qtz. syenite-2	112.4	57.97	5.61	0.727423	0.000008	0.70475	9.61	62.43	0.0931	0.51232	5	−6.2	−0.53	−2.5	1049
5	B425	granite	186.8	46.97	11.53	0.749261	0.000007	0.70431	2.09	14.73	0.0861	0.512339	4	−5.8	−0.56	−1.9	969
6	A447-4	comendite	270.6	38.61	20.4	0.786143	0.000008	0.70662	21.81	116.14	0.1135	0.512375	4	−5.1	−0.42	−2.2	1178
7	B382-2	comendite	282.3	14.16	58.9	0.933767	0.000008	0.70813	15.35	76.07	0.122	0.512361	4	−5.4	−0.38	−2.7	1310
8	B382-1	comendite	233.3	19.28	35.49	0.85144	0.00009										
9	B385	trachyandesite	112.2	620	0.523	0.708063	0.000007	0.70602	5.93	34.36	0.1043	0.512295	5	−6.7	−0.47	−3.4	1190
10	B386	trachyandesite	124.8	638.6	0.564	0.707993	0.000006	0.70579	5.77	33.04	0.1055	0.51229	5	−6.8	−0.46	−3.5	1211
Tsagan–Khurtie Range (210 Ma)																	
11	B440	comendite	216.5	19.36	32.57	0.789441	0.000008	0.70238	11.43	61.28	0.1128	0.51267	4	0.6	−0.43	2.9	726
12	B444	comendite	135.1	18.19	21.57	0.763315	0.000008	0.70557	18.74	100.5	0.1127	0.512676	4	0.7	−0.43	3.0	716
13	1/8	comendite	162	12.2	38.87	0.82044	0.00023	0.7032	12.1	66.7	0.1099	0.512625	7	−0.3	−0.44	2.1	771
14	1/6	trachybasalt	12.7	988	0.037	0.70455	0.00015	0.7044	6.09	30.09	0.1192	0.512632	7	−0.1	−0.39	2.0	836
15	1/7	trachybasalt	10	1188	0.024	0.70506	0.00012	0.7049	7.22	37.4	0.1168	0.512646	7	0.2	−0.41	2.3	793
16	B446-1	trachybasalt	16.9	1136	0.04	0.704339	0.000008	0.70422	8.08	41.09	0.1189	0.512694	4	1.1	−0.4	3.2	734

(1) Analyses performed at Universite de Rennes 1, except sample 8 that was analyzed at the Geological Institute (Ulan-Ude) and samples 13–15, which were analyzed by Yarmolyuk et al. (2001).
(2) NBS 987 Sr standard = 0.710250; VNIIM Sr standard = 0.70801.
(3) Errors in $^{87}Sr/^{86}Sr$ are 2σ (in-run precision). $(^{87}Sr/^{86}Sr)_T$ is 2σ propagated to include individual within-run error, reproducibility of standard analyses, and uncertainty in Rb/Sr ratios.
(4) AMES ND standard = 0.511965. Errors in $^{143}Nd/^{144}Nd$ are 2σ, based on within-run statistics. Errors in $\varepsilon_{ND}(T)$ are 2σ propagated to include individual within-run error, reproducibility of standard analyses and uncertainty in Sm/Nd ratios.

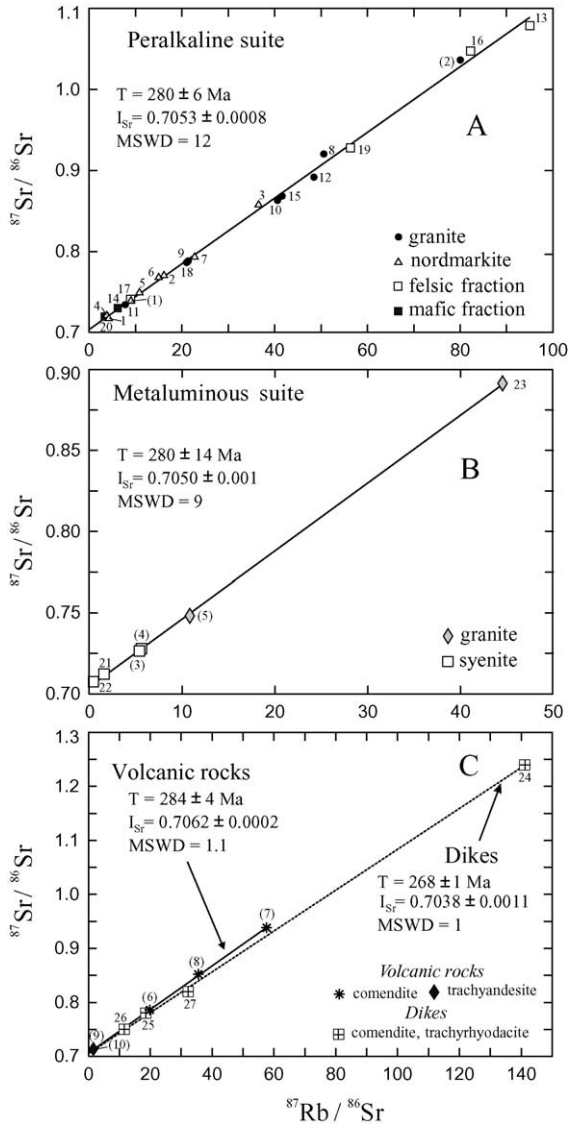

Fig. 6. Rb–Sr isotope diagrams (A, B, C) of plutonic and volcanic rocks from the Bryansky Complex. Sample numbers as in Table 5 and in Table 6 (in parentheses). Felsic and mafic fractions are mainly alkali feldspar and Amph + Cpx, respectively.

was performed mainly in porphyritic varieties. This allowed estimates of both liquidus and solidus temperatures (T_L and T_S). We assumed that liquidus temperature could be estimated by the homogenization temperature (T_h) of melt inclusions in the core of large phenocrysts, whereas near-solidus temperatures could be obtained from the T_h in groundmass quartz grains.

Assessment of T_L in syenitic magmas was fraught with difficulties due to the absence of melt inclusions in subliquidus alkali feldspar grains. However, a rough estimation of the liquidus temperature of nordmarkite magma was obtained by determination of T_h of melt inclusions in pyroxene from a fine-grained syenite that shows a 5–7-cm-wide chilled zone near the contact of nordmarkite-1 with metamorphic roof pendant. Interaction between magma and carbonate-rich country rock caused formation of pyroxene in nordmarkite-1. In the pyroxene grains, numerous melt inclusions have been found. These inclusions are supposed to establish the lower limit of liquidus temperature in the peralkaline syenite melt.

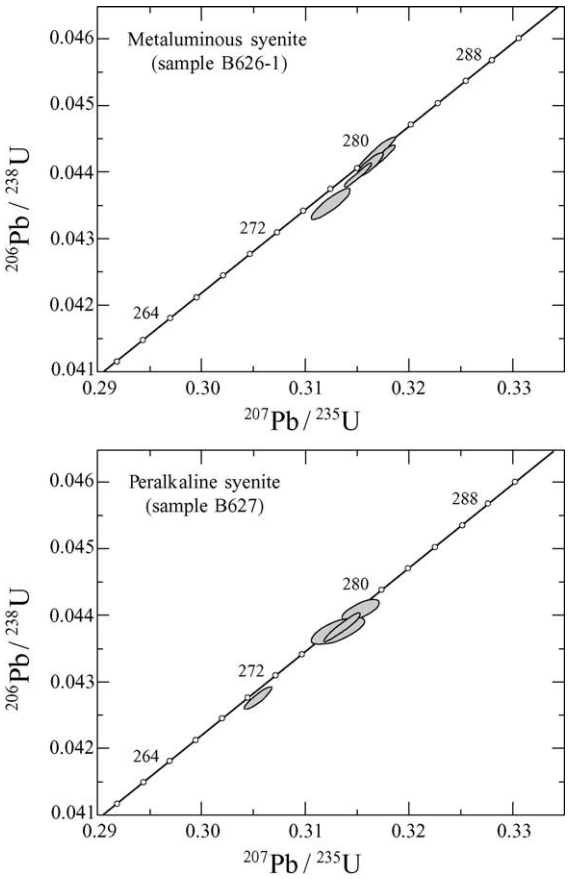

Fig. 7. U–Pb Concordia diagram of multigrain zircon analyses. A = metaluminous quartz syenite (sample B626-1); B = nordmarkite (sample B627).

The main results obtained from microthermometric study are given in Table 7. The data show that T_L in peralkaline syenitic and granitic magmas are significantly different, ≥940 and 760–790 °C, respectively. In granite, T_S was about 680–700 °C. In quartz phenocrysts from comendite, T_S is similar to that in granite, whereas T_L varied widely, from 850 °C to almost 1100 °C. Since the T_h values of about 1000–1100 °C look anomalously high for silicic rocks, the reliability of data obtained should be discussed.

It has been known that homogenization temperature of MI is comparable with the true temperature of the captured melt, only if the inclusion remains intact. However, melt inclusions can be affected by processes such as volatile dissociation, degassing, oxidation and/or partial re-equilibration with their host, both during natural cooling and homogenization experiments (Roedder, 1984; Qin et al., 1992; Lu et al., 1995; Nakamura and Shimakita, 1998; Danyushevsky et al., 2002).

Experimental study and modeling showed that the time span that is required for complete re-equilibration is very small in the geological scale of time (Qin et al., 1992; Hall and Sterner, 1993). Consequently, if the re-equilibration processes seriously affect the system 'melt inclusion-host', the fluid content in melt inclusions (and consequently, the homogenization temperature) is expected to be more or less similar throughout the crystal. Our data on systematic decrease of T_h in melt inclusions from the core to margins of zoned phenocrysts suggest that H_2O loss did not play a great role in the given case. Similar conclusions can be made from the results obtained by Wilding et al. (1993). These authors revealed that, in spite of significant degassing of rhyolite melt during or prior the eruption, the H_2O concentration in the trapped glass (melt inclusions) within the phenocrysts proved to be high and corresponded to the water-saturated level.

To minimize the effect of the processes that manifest themselves during the homogenization experiments, we proceeded from the data that the fluid loss extent depends significantly on the inclusion size (e.g., Student and Bodnar, 1999). Heating of melt inclusions ≥10 μm in diameter usually causes partial loss of the fluid phase, and this resulted in higher temperature of their homogenization (Kravchuk et al., 1992; Student and Bodnar, 1999). Our study also showed that melt inclusions ≥10 μm in quartz phenocrysts from comendite contained about 2 wt.% H_2O before heating (ion probe analysis), but after homogenization, water in such inclusions was not recorded at all or constitute of about 0.5 wt.% (Kuzmin et al., 1999). As for the T_h value in these larger melt inclusions, it proved to be 50 °C higher than in small ≤5 μm inclusions. That is why, according to Reyf et al. (1994) recommendations, we determined T_h values in melt inclusions of 1–3 μm in size that are located mainly within the crystal core (see Analytical methods). For the above considerations, it is believed that the approaches used for the melt inclusion study provided reliable estimates of trapping temperature of the host magma both in plutonic and volcanic rocks.

The results of microprobe analyses of homogenized melt inclusions are reported in Table 8. The homogenized melt inclusions are shown to have similar compositions to the host rock, and, in doing so, indicate the reliability of data on T_h obtained in studies of melt inclusions. The observed differences can be readily explained by the microprobe analysis technique of elements determination in the small, about 10 μm inclusions (in particular, loss of Na).

Table 7
The homogenization temperature (T_h, °C) of melt inclusions in quartz and clinopyroxene from plutonic and volcanic rocks

Rock	Sample number	Crystal-1	Crystal-2 and outer zone of Crystal-1	Matrix
Nordmarkite *	B527-6	930–940		
Peralkaline granite	B389	760–790		700–720
	B388		700–720	680–700
	A444			700–710
Comendite	M250-7	1100		
	B603-4	1090		
	B600-1	1090		
	A447-7	980–1020		
	A447-5	920–930	700–710	660–680
	B382-2	850–880	820–840	
	A452-1	860–880	840–860	
	A451-4		700–720	

(1) Crystal-1 and Crystal-2 = large and small phenocryst, respectively.
(2) Asterisk = melt inclusions in pyroxene, the rest are in quartz.

Table 8
Composition of homogenized melt inclusions (MI) and host rocks (WR) (wt.%)

Rock	Nordmarkite						Peralkaline granite						Comendite	
Sample no.	B527-8			A444			B388			B389			B600-1	
	MI			WR	MI		WR	MI		WR	MI		MI	
SiO_2	72.73	71.03	68.68	74.9	76.13	71.76	72.6	72.11	72.77	74.4	76.54	73.09	75.95	75.85
TiO_2	0.06	0.04	0.05	0.23	0.21	0.19	0.3	0.6	0.68	0.21	0.42	0.42	0.22	0.32
Al_2O_3	11.41	13.38	13.72	12.1	10.02	12.47	12	8.67	8.62	10.6	8.66	8.72	10.8	10.24
FeO *	1.03	1.11	1.37	2.29	1.65	1.73	3.75	2.8	2.37	4.29	2.54	2.69	3.17	3.25
MnO	0.08	0.07	0.11	0.03	0.08	0.05	0.11	0.26	0.24	0.19	0.23	0.35	0.24	0.23
MgO	0.29	0.47	0.24	0.12	0.01	0.05	0.23	0.06	0.04	0.21	0.05	0.02	0.07	0.06
CaO	1.77	1.65	1.29	0.18	0.12	0.01	0.15	0.06	0.03	0.5	0.08	0.06	0.1	0.12
Na_2O	2.35	3.32	2.59	4.1	2.37	4.85	4.76	4.25	3.45	4.21	2.42	2.06	2.92	2.56
K_2O	4.26	4.75	4.94	5.26	3.41	4.72	4.74	3.36	3.67	4.6	3.88	4	3.42	3.15
LOI	n.d.	n.d.	n.d.	0.53	n.d.	n.d.	0.97	n.d.	n.d.	0.84	n.d.	n.d.	n.d.	n.d.
F	–	–	–	n.d.	1.71	1.47	n.d.	1.71	1.1	n.d.	1.7	1.52	0.69	0.63
C1	0.24	0.2	0.33	n.d.	0.19	0.07	n.d.	0.28	0.22	n.d.	0.23	0.29	0.19	0.18
Total	94.22	96.02	93.32	99.74	95.9	97.37	99.61	94.06	93.19	100.1	96.75	93.22	97.77	96.59

Rock	Comendite															
Sample no.	M250-7			B603-4			A447-7			B383-3			A451-4		A447-5	
	WR	MI		WR	MI		WR	MI		WR	MI		MI		MI	
SiO_2	74.68	75.83	75.18	73.6	73.47	72.71	74.34	75.75	75.62	72.91	74.5	74.76	73.09	75.12	75.92	73.11
TiO_2	0.48	0.26	0.5	0.49	0.17	0.21	0.48	0.23	0.43	0.47	0.08	0.42	0.21	0.16	0.13	0.27
Al_2O_3	10.4	9.32	9.54	10.5	11.25	9.82	10.71	10.35	9.3	12.27	12.65	9.49	12.12	9.89	9.53	11.07
FeO *	3.99	3.23	3.45	4.46	3.19	3.98	4.24	2.41	5.22	3.71	1.25	3	0.68	1.09	0.67	0.93
MnO	0.24	0.23	0.26	0.19	0.25	0.22	0.18	0.15	0.24	0.11	0.27	0.23	0.07	0.09	0.07	0.12
MgO	0.04	0.08	0.06	0.14	0.09	0.1	0.12	0.06	0.12	0.05	0.08	0.05	0.05	0.04	0.01	0.03
CaO	0.15	0.13	0.17	0.42	0.14	0.17	0.24	0.12	0.16	0.07	0.23	0.12	0.2	0.15	0.01	0
Na_2O	3.89	2.78	3.07	4.08	2.14	1.67	4.14	1.48	2.13	3.5	3.74	3.01	2.79	2.77	2.91	3.88
K_2O	4.49	5.15	4.51	4.4	5.65	5	4.39	6.08	3.56	5.41	5.63	4.24	4.6	4.14	3.13	4.62
LOI	0.87	n.d.	n.d.	1.46	n.d.	n.d.	0.62	n.d.	n.d.	1	n.d.	n.d.	n.d.	n.d.	n.d.	n.d.
F	n.d.	–	–	n.d.	–	–	n.d.	–	–	n.d.	–	–	0.59	0.91	1.59	1.85
Cl	n.d.	0.04	0.23	n.d.	0.67	0.63	n.d.	0.22	0.3	n.d.	0.39	0.34	0.23	0.21	0.27	0.07
Total	99.23	97.05	96.97	99.74	97.02	94.51	99.46	97.05	96.97	99.5	99.88	95.89	94.61	94.57	94.23	95.95

(1) In melt inclusions, the detection limit for all components is 0.05–0.7 wt.%; for F < 0.3 and < 0.15 wt.% in plutonic and volcanic rocks, respectively.
(2) FeO * = total Fe calculated as FeO.

The data on melt inclusion composition indicate that peralkaline magmas contained enhanced Cl (about 0.2–0.3 wt.%), which did not change from early to late stages. By contrast, the distribution of F is uneven. In nordmarkite it was low, less that the detection limit (≤ 0.3 wt.%), while in peralkaline granite magma, F content was 1.5–1.7 wt.%. In comendite melts, F had a wide range of concentration, from below the detection limit to 1.5 wt.%. Melt inclusions with high T_h values have F ≤ 0.69 wt.% (samples B603-4 and B600-1), whereas in melt inclusions with lower $T_h = 920–930$ °C (sample A447-5) the F contents is higher (>1.5 wt.%), similar to those in granites.

7. Discussion

It follows from the above description that the plutonic rocks of the Bryansky Complex possess all the main features characteristic of A-type granites (Loiselle and Wones, 1979; Whalen et al., 1987; Eby, 1990, 1992). They formed during the anorogenic stage of the mobile belt evolution, within the intra-

continental rift zone, and consist of perthitic alkali feldspar and quartz, with Na-rich amphibole and pyroxene or Fe-rich biotite. The granitoids are highly enriched in alkalis and HFSE; granites from both suites are impoverished in Sr and Ba.

Crosscut relations of magmatic rocks point to the following sequence: metaluminous suite–bimodal volcanic suite–peralkaline suite. At the same time, U–Pb zircon dating and Rb–Sr whole-rock dating testify that formation of the Bryansky Complex occurred during a short time span, about 280 ± 4 Ma. Close association of magmatic suites in space and time is accompanied by striking similarity of isotope data. The $\varepsilon_{Nd}(T)$ values in all rock types (except trachyandesites) range from -1.9 to -3.0, with total overlap of data from different suites within the error limit (Table 6). The $(^{87}Sr/^{86}Sr)_T$ values are also similar (Fig. 6). All above data suggest consanguinity of main rock types making up the Bryansky Complex. Below, based on this conclusion, we are discussing some particular problems concerning the relations of various suites and various rock types within the suites.

7.1. The role of fractional crystallization during the formation of syenite–granite suites

The metaluminous and the peralkaline suites evolved from syenite to quartz syenite to granite (Table 4; Figs. 2–5). This could be caused by two processes: (1) fractional crystallization of syenitic magmas and (2) assimilation of silica-rich crustal material by syenite melts. In the light of available isotope data, the second model looks less realistic. This is especially clear from the comparison of $\varepsilon_{Nd}(T)$ values (Table 6): even if the error limit is not taken into account, it is seen that syenites in both suites have higher negative $\varepsilon_{Nd}(T)$ values than granites. Consequently, granitic melts cannot be interpreted as products of the lower crust material assimilation by the syenite magma. Assimilation of crustal material could occur during the early syenite magma formation, but there are not data on contemporaneous mantle-derived mafic rocks to check this suggestion.

The fractional crystallization model explains all the main features of the syenite–granite suites' evolution. In particular, the decrease of Ca, Mg, Ti, Na, K, Ba, and Sr with simultaneous increase of Rb going from syenites to granites (Figs. 2 and 4) is consistent with the separation of feldspars, mafic and Fe–Ti oxide minerals. Separation of alkali feldspar is supported by the data on cumulus feldspar crystal presence in metaluminous syenite and probably nordmarkite. Enrichment of the peralkaline granite in F, as compared to earlier nordmarkite, is also consistent with the fractional crystallization model. The REE patterns in magmatic rocks suggest fractionation of some accessory minerals as well. In the metaluminous suite, systematic decrease of REE content could be caused by settling of titanite, whereas zircon was fractionated later, at the granitic stage (Fig. 3). In the peralkaline suite, significant decrease of REE content, along with Th, occurred only at the granite stage (Figs. 4 and 5). Since concentration of Zr, Nb, Y and Hf in the granite remained at the same level as in the nordmarkite-2, it is likely that REE and Th at this stage were removed mainly by monazite.

7.2. Relationship between the metaluminous and peralkaline suites

The metaluminous and peralkaline suites are of similar age and share a number of important traits, including isotope characteristics. Since the metaluminous rocks preceded the peralkaline granitoids, and since the syenites are parental for all the rest of the granitoids in each suite, a question arises: is it likely that metaluminous syenite was parental also for nordmarkite? When comparing average chemical compositions of metaluminous syenite-1 and nordmarkite-1, a regular distinction can be seen. Nordmarkite contains less Sr, Rb, Ba, Th, Ta, Zr, Hf, Ca, and total REE (Fig. 8, Table 4). These distinctions can be readily explained by separation of alkali feldspar and some accessories from the metaluminous syenite magma (or, alternatively, by partial melting of already crystallized syenite). This assumption is supported by least-square modeling of fractional crystallization (Table 9): separation of ~ 25 wt.% alkali feldspar and 1.5% Fe–Ti oxides and titanite should produce $\sim 75\%$ of residual melt of nordmarkite composition.

7.3. A correlation of comendites with peralkaline granites

Comendites and peralkaline granites have similar age and Sm–Nd isotope characteristics (Fig. 6 and

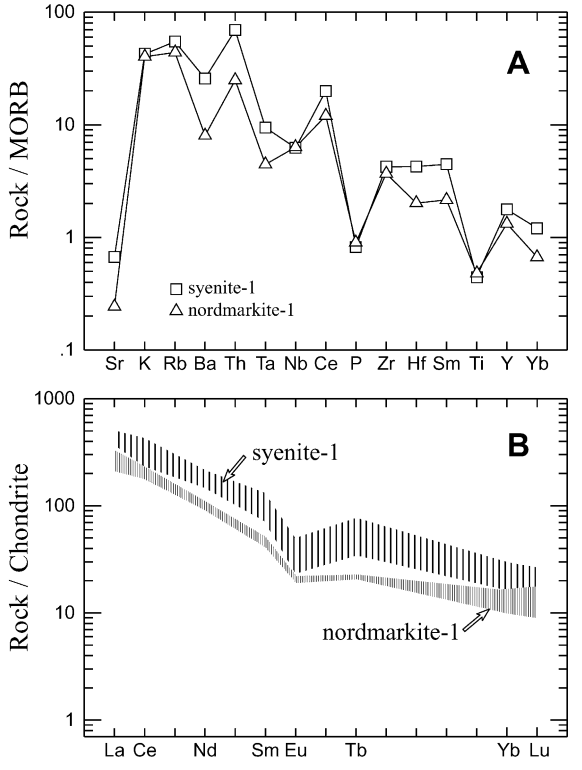

Fig. 8. Concentration of trace elements in average syenite-1 and nordmarkite-1. A = MORB-normalized spidergram; B = Chondrite-normalized REE abundance. MORB values are from Pearce (1983), chondrite values are from Sun and McDonough (1989).

Table 6). These rock types are indistinguishable in major and trace element contents, except some HFSE (Fig. 4). This suggests that comendites are extrusive analogue of peralkaline granite and, like granite, formed as a result of fractional crystallization of nordmarkite magma. The difference could be caused by weak settling of accessory minerals during the comendite magma formation (Fig. 9).

The least-square modeling shows that a residual melt of comendite composition can be produced by fractionation of ~80 wt.% alkali feldspar and about 6 wt.% amphibole, Fe–Ti oxides and apatite from the nordmarkite magma (Table 9). Given the large amount of estimated crystal phase, it is suggested that the residual silicic magma is the result of separation rather than crystal settling in a magma chamber.

7.4. Temperatures of crystallization and generation of peralkaline silicic magmas

The melt inclusion study gave a liquidus temperature of syenite magma in excess of 930–940 °C. Granitic melts started to crystallize at 760–790 °C, while their near-solidus temperature was 700–720 °C (Table 7). The comparatively narrow, 60–70 °C, solidus-to-liquidus temperature range in granite magma was probably caused by enrichment in volatiles, F (up to 1.5–1.7 wt.%, see Table 8) and H_2O. Estimation of water content in granite magma can be made, as a first approximation, using a diagram with liquidus curves for a given amount of H_2O in the natural subaluminous granite system (Holtz et al., 2001). As granite intrusions are related to the volcanic suite and commonly contain abundant miarolitic cavities, we can suggest a shallow depth of magma crystallization. According to that diagram, at a tem-

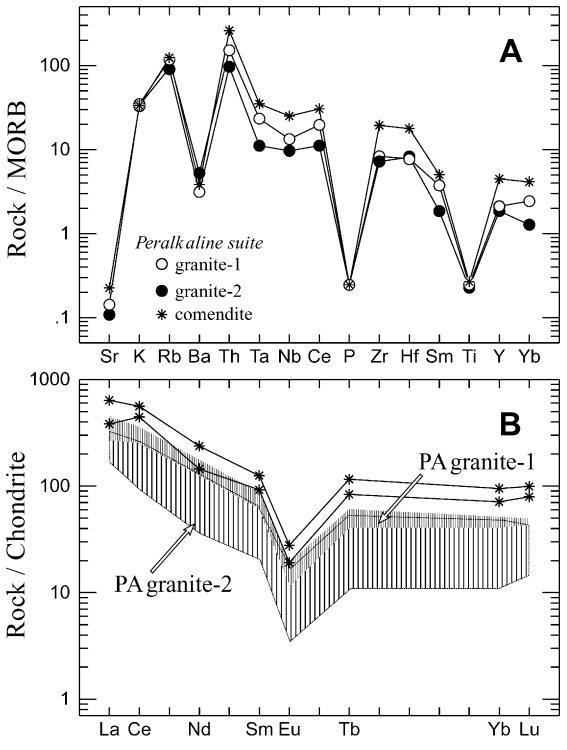

Fig. 9. Concentration of trace elements in average comendites and peralkaline granites. A = MORB-normalized spidergram; B = Chondrite-normalized REE abundance. MORB values are from Pearce (1983), chondrite values are from Sun and McDonough (1989).

Table 9
Results of least-square modeling of fractional crystallization

	Nordmarkite-1—Comendite			Syenite-1—Nordmarkite-1		
	Parent	Daughter	Calculated	Parent	Daughter	Calculated
SiO_2	64.97	73.63	73.62	64.06	64.98	64.90
TiO_2	0.70	0.42	0.42	0.69	0.70	0.65
Al_2O_3	16.38	11.60	11.84	17.19	16.39	16.95
FeO *	3.16	3.77	3.77	3.26	3.16	3.16
MnO	0.12	0.13	0.28	0.11	0.12	0.15
MgO	0.44	0.15	0.00	0.44	0.44	0.60
CaO	0.53	0.08	0.32	0.77	0.53	0.71
Na_2O	6.36	4.27	4.44	5.99	6.36	6.03
K_2O	6.20	4.91	4.21	6.38	6.20	5.84
P_2O_5	0.10	0.03	0.00	0.10	0.10	0.14
Rb	99	238	189	102	99	133
Ba	149	51	42	589	149	269
Sr	29	21	9	98	29	31
Zr	459	1717	1415	319	459	430
Fractionating minerals (wt.%)	Alkali feldspar		78.6			24.4
	Fe–Ti oxides		2.2			0.9
	Amphibole		3.9			–
	Apatite		0.3			–
	Titanite		–			0.5
Residual melt (wt.%)			15.0			74.1
Sum residuals squared			0.776			0.627

(1) Major elements are recalculated to total= 100% volatile free; total Fe as FeO.
(2) For the least-square modeling, mineral compositions (Table 1, samples 1 and 5; Table 2, sample 6) and average rock compositions were used; samples with cumulate phase were not included in the averages calculations.
(3) Partition coefficients for model "Nordmarkite-1—Comendite" are from Mahood and Hildreth (1983), Arth (1976), Pearce and Norry (1979), and from Mahood and Stimac (1990) for model "Syenite-1—Nordmarkite-1".

perature in the range 760–790 °C and a pressure ≤ 2 kbar, the minimum amount of water in the granite magma was about 2–4 wt.%.

The data obtained characterize temperature conditions at/near the pluton formation level, but they do not necessary provide an answer to the question what was the magma generation temperature in the source region. This information can hardly be derived from studies of melt inclusions from plutonic rocks. However, the magma generation temperature may be estimated by study of melt inclusions in quartz phenocrysts from comendites, the volcanic counterparts of granite. This suggestion is based upon the following considerations.

The A-type granites crystallized from magmas that were generated at great depth and characterized by low water content ≤ 3 wt.% (Clemens et al., 1986; Reyf and Bazheev, 1985; Vielzeuf et al., 1990). In granitic magmas impoverished in H_2O, quartz is a liquidus mineral (Stern et al., 1975). Hence, it follows that the intratelluric quartz crystals formed at the melt generation level could contain melt inclusions captured by growing crystals within or near the magma chamber. However, it is unlikely that such early crystals could persist in plutonic rocks since in the course of slow magma ascent they should be resorbed and/or recrystallized. To the authors' knowledge, the only well documented high T_h, up to 1045 ± 13 °C, was established by Reyf (1997) in the Cl-rich and H_2O impoverished A-type granite pluton in Transbaikalia, Russia. Much more information in this respect can be obtained from the extrusive counterparts in which early crystals might be preserved owing to rapid solidification of silicic magma. As this extrusive magma ascends, its crystallization continues, therefore quartz phenocrysts formed at different

depths (and at different temperatures) may be present in the same sample. This is why only those melt inclusions in phenocryst cores that have the highest temperature of homogenization can be considered as the most representative for assessing the magma generation temperature.

The highest values of T_h, up to 1100 °C (Table 7), were determined in quartz phenocryst cores from comendite samples. These results suggest that the temperature of comendite (and peralkaline granite) magma *generation* was about 1100 °C. Consequently, the parental syenite melts should be generated at still higher temperature.

Such a high temperature of comendite magma generation is not unique. In the bimodal trachybasalt–comendite series of the Tsagan–Khurtei Range situated in the neighbouring area, the maximum T_h value in the quartz phenocrysts from comendite is 1030–1100 °C with total H_2O and F content in melt inclusions ≥ 1 wt.% (determined by ion and electron microprobe analysis, Kuzmin et al., 1999). In quartz phenocrysts from pantellerite from the Pantelleria Island, the T_h of melt inclusions is even higher, up to 1135 °C (Kovalenko et al., 1994). Similar order of T_h is reported for alkaline rhyolites from many other localities in the world (see compilation in Litvinovsky, 1990).

The data on the very high temperature of silicic magmas has produced a resurgence of interest in the problem of the great depth of its generation (Litvinovsky et al., 2000). From the experimental data, it is known that if the liquidus temperature of granitic or haplogranitic magma amounts to 1000–1100 °C, and this magma contains about 1–2 wt.% H_2O, it would require a pressure of 15 kbar or more (Stern et al., 1975; Huang and Wyllie, 1975; Johannes and Holtz, 1996; Holtz et al., 2001). When the fluid phase also contains CO_2, the pressure would be even higher (Keppler, 1989). Authors realize that high-pressure experimental results were obtained in subaluminous granite and haplogranite, so that the liquidus curves in the comendite–H_2O system are not necessary the same. However, melting experiments performed by Scaillet and McDonald (2001) with three peralkaline rhyolites show that liquidus curves for 1 and 2.5 wt.% H_2O content are shifted at ~ 100 °C to the lower temperature field of PT-diagram at pressure of 0.5 and 1.5 kbar. This suggests that liquidus temperature of about 1000–1100 °C in comendite magma with low water content may correspond to similar or even higher pressure than in subaluminous granite system. Temperature estimates from dehydration melting of biotite and amphibole bearing tonalitic rocks support this conclusion. Silicic magmas approximating compositionally A-type granite formed at 1 kbar within a temperature range of 830–900 °C (Clemens et al., 1986); at 6–8 kbar the temperature increased to 900–950 °C (Creaser et al., 1991; Patiño Douce, 1997); at 10 kbar it reached 1000 °C (Skjerlie and Johnston, 1992) and at 15–25 kbar it was 1100–1150 °C (Litvinovsky et al., 2000). When considering the possible depth of the Bryansky Complex silicic magma generation, we conclude that temperatures of 1000–1100 °C are approximately the highest recorded in the continental crust (Kilpatrick and Ellis, 1992; Rudnick, 1992; Downes, 1993). They exceed the conventional higher limit of the granulite metamorphic grade in the lower crust. Temperatures as high as this are characteristic of some very high-pressure (≥ 14 kbar) granulite lithologies formed at great depth (e.g., Del Lama et al., 2000; see also references in Litvinovsky et al., 2000). It follows that A-type granite magmas could form at the base of thickened (up to 60–70 km) continental crust or even at a greater depth. A similar hypothesis was suggested by Whalen et al. (1996) for A-type granites from the Topsails igneous suite, Newfoundland Appalachians. These authors assumed that the granite magma was produced by remelting of hybridized lithospheric mantle, and the granites might recycle previously subducted continental material.

7.5. Provenance of silicic magmas

The foregoing petrogenetic analysis has demonstrated that all silicic rocks from the Bryansky Complex are genetically related. The metaluminous syenite magma was probably parental to the whole complex. If this is the case, common silica oversaturated crustal lithologies would not be a likely source. It was established that, contrary to the conclusion of Huang and Wyllie (1981), melting of such rocks even at very high pressure (15 to 25 kbar) leads to the formation of granitic rather than syenitic magmas (Litvinovsky et al., 2000). In addition, the very high alkali content in

syenite (about 12–13 wt.%) implies that the source rocks were high in alkalis, and not just impoverished in silica. Thus, two possible types of source rocks can be envisioned: (i) crustal lithologies of intermediate or basic composition strongly enriched by alkali-rich fluids, and (ii) metasomatised mantle rocks enriched in alkalis (or, alternatively, alkali-rich basalt magmas). Our Rb–Sr and Nd–Sm isotope data suggest that the dominant role of mantle-derived material is more probable.

Fairly low $(^{87}Sr/^{86}Sr)_T$ values for all rock types of the Bryansky Complex (0.7040–0.7060) suggest a significant contribution of mantle-derived material in the silicic magmas (Fig. 6). The $\varepsilon_{Nd}(T)$ values ranging from −2 to −3.5, indicate, along with $(^{87}Sr/^{86}Sr)_T$ data, that the granitoid rock compositions tend to be located in the vicinity of Mantle Array in the $\varepsilon_{Nd}(T)$ vs. $(^{87}Sr/^{86}Sr)_T$ diagram. Taking into consideration that the $\delta^{18}O$ values in peralkaline syenites and granites range from +5.5 to +6 (Wickham et al., 1995, 1996), we can conclude that the most plausible source for granitoid melts was enriched mantle. The high temperature of the silicic magmas (1000–1100 °C), characteristic of the mantle or the base of overthickened crust, supports the dominant role of the mantle in the Bryansky granitoids and comendite formation. Indirect evidence that comendite magmas could be generated from the mantle-derived material was obtained by the Sr–Nd study of trachybasalts and comendites from younger, Triassic bimodal suite. This suite is also located within the Mongolian–Transbaikalian Belt, about 200 km to the east, in the Tsagan–Khurtei Range. The Nd–Sr isotope data (Table 6) demonstrate a close link of comendites and mantle-derived K-rich basalts to the mantle source, although in this case it was more likely depleted rather than enriched mantle.

8. Conclusions

(1) The evolution of the two magmatic suites making up the Bryansky Complex was defined mainly by fractional crystallization of syenitic and nordmarkitic magmas respectively. Metaluminous syenite magmas are considered to be parental to the entire Bryansky Complex.

(2) Rb–Sr and Sm–Nd isotope data suggest the dominant role of a mantle-derived source, from which metaluminous and peralkaline granitoid magmas were derived. The juvenile nature of the voluminous granitoids supports the idea of significant crustal growth in the Phanerozoic in Central Asia (Kovalenko et al., 1996; Jahn et al., 2000).

(3) The unusually high homogenization temperature of melt inclusions in the quartz phenocrysts from comendite suggests a very high temperature (about 1000–1100 °C) of magma generation which could occur at great depths exceeding the normal crust thickness.

(4) Since the Bryansky Complex represents a typical A-type granite belt formed in the planetary scale network of intracontinental rift zones of Central Asia, the above conclusions may shed light on the genesis of A-type granitoids related to intracontinental rifting.

Acknowledgements

The Russian Foundation of Basic Researches grants awarded to BAL (99-05-65138) and ANZ (97-05-96355) supported this contribution. BmJ was supported by the INSU-CNRS through the Programme "Dinamique des Transferts Terrestress" (1997–1998) and "Interieur de la Terre" (1998–1999). This is a contribution to IGCP-420: Crustal growth in the Phanerozoic: Evidence from Central Asia. Constructive reviews by G.N. Eby and C. Villaseca have substantially improved the final draft. Authors also grateful to F.G. Reyf for valuable discussions. **[EO]**

References

Anderson, J.L., Morrison, J., 1992. The role of anorogenic granites in the Proterozoic crustal development of North America. Dev. Precambrian Geol. 10, 263–299.

Arth, J.G., 1976. Behavior of trace elements during magmatic processes—a summary of theoretical models and their applications. J. Res. U.S. Geol. Surv. 4, 41–47.

Bailey, D.K., 1978. Continental rifting and mantle degassing. In: Neumann, E.R., Ramberg, I.B. (Eds.), Petrology and Geochemistry of Continental Rifts. D. Reidel Publishing Company, Oslo, pp. 1–13.

Barker, F., Wones, D.R., Sharp, W.N., Desborough, G.A., 1975. The Pikes Peak batholith, Colorado Front Range, and a model for the origin of the gabbro–anorthosite–syenite–potassic granite suite. Precambrian Res. 2, 97–160.

Black, P.M., Brothers, R.N., Yokoyama, K., 1988. Mineral parageneses in eclogite-facies meta-acidites in northern New Caledonia. In: Smith, D.C. (Ed.), Eclogites and Eclogite-Facies Rocks. Development in Petrology, vol. 12. Elsevier, Amsterdam, pp. 271–290.

Clemens, J.D., Holloway, J.R., White, A.J.R., 1986. Origin of an A-type granite: experimental constraints. Am. Mineral. 71, 317–324.

Collins, W.J., Beams, S.D., White, A.J.R., Chappell, B.W., 1982. Nature and origin of A-type granites with particular reference to Southeastern Australia. Contrib. Mineral. Petrol. 80, 189–200.

Corfu, F., Noble, S.R., 1992. Genesis of the southern Abitibi greenstone belt, Superior Province, Canada; evidence from zircon Hf isotope analyses using a single filament technique. Geochim. Cosmochim. Acta 56, 2081–2097.

Creaser, R.A., Price, R.C., Wormald, R.J., 1991. A-type granites revisited: assessment of a residual-source model. Geology 19, 63–166.

Danyushevsky, L.V., McNeill, A.W., Sobolev, A.V., 2002. Experimental and petrological studied of melt inclusions in phenocrysts from mantle-derived magmas: an overview of techniques, advantages and complications. Chem. Geol. 183, 5–21.

Del Lama, E.A., Zanardo, A., Oliveira, M.A.F., Morales, N., 2000. Exhumation of high-pressure granulites of the Guaxupè Complex, Southeastern Brazil. Geol. J. 35, 231–249.

Downes, H., 1993. The nature of the lower continental crust of Europe: petrological and geochemical evidence from xenoliths. Phys. Earth Planet. Inter. 79, 195–218.

Eby, G.N., 1990. The A-type granitoids: a review of their occurrence and chemical characteristics and speculations on their petrogenesis. Lithos 26, 115–134.

Eby, G.N., 1992. Chemical subdivision of the A-type granitoids: petrogenetic and tectonic implications. Geology 20, 641–644.

Gordienko, I.V., 1987. Paleozoic Magmatism and Geodynamic Regime in Central-Asian Folded Belt. Nauka, Moscow, USSR, 237 pp. (in Russian).

Hall, D.L., Sterner, S.M., 1993. Preferential water loss from synthetic fluid inclusions. Contrib. Mineral. Petrol. 114, 489–500.

Harris, N.B.W., Marzouki, F.M.H., Ali, S., 1986. The Jabel Sayid complex, Arabian shield: geochemical constraints on the origin of peralkaline and related granites. J. Geol. Soc. (Lond.) 143, 287–295.

Hayob, J.L., Essene, E.J., Ruiz, J., Ortega-Guitierrez, F., Aranda-Gomez, J.J., 1989. Young high-temperature granulites from the base of the crust in central Mexico. Nature 342, 265–268.

Holtz, F., Johannes, W., Tamic, N., Behrens, H., 2001. Maximum and minimum water contents of granitic melts generated in the crust: a reevaluation and implications. Lithos 56, 1–14.

Huang, W.L., Wyllie, P.J., 1975. Melting reactions in the system $NaAlSi_3O_8$–SiO_2 to 35 kilobar, dry and with excess water. J. Geol. 83, 737–748.

Huang, W.L., Wyllie, P.J., 1981. Phase relationship of S-type granite with H_2O to 35 kbar: muscovite granite from Harney Peak, South Dakota. J. Geophys. Res. 86, 10515–10529.

Jaffey, A.H., Flynn, K.F., Glendenin, L.E., Bentley, W.C., Essling, A.M., 1971. Precision measurement of half-lives and specific activities of ^{235}U and ^{238}U. Phys. Rev., C Nucl. Phys. 4, 1889–1906.

Jahn, B.M., Cornichet, J., Cong, B.L., Yui, T.F., 1996. Ultrahigh-ε_{Nd} eclogites from an ultrahigh-pressure metamorphic terrane of China. Chem. Geol. 127, 61–79.

Jahn, B.M., Wu, F., Chen, B., 2000. Granitoids of the Central Asian Orogenic Belt and continental growth in the Phanerozoic. Trans. R. Soc. Edinb. Earth Sci. 91, 181–193.

Johannes, W., Holtz, F., 1996. Petrogenesis and Experimental Petrology of Granitic Rocks. Springer, Berlin, 330 pp.

Keppler, H., 1989. The influence of the fluid phase composition on the solidus temperatures in the haplogranite system $NaAlSi_3O_8$–$KalSi_3O_8$–SiO_2–H_2O–CO_2. Contrib. Mineral. Petrol. 102, 321–327.

Kerr, A., Fryer, B.J., 1993. Nd isotope evidence for crust–mantle interaction in the generation of A-type granitoid suites in Labrador, Canada. Chem. Geol. 104, 39–60.

Kilpatrick, J.A., Ellis, D.J., 1992. C-type magmas: igneous charnockites and their extrusive equivalents. Trans. R. Soc. Edinb. Earth Sci. 83, 155–164.

Kovalenko, V.I., Naumov, V.B., Solovova, I.P., Girnis, A.V., Hervig, R.L., Boriani, A., 1994. Volatiles, composition and conditions of crystallization of magmas formed basalt–pantellerite association at Pantelleria Island (by study of melt and fluid inclusions). Petrologia 2, 24–42 (in Russian).

Kovalenko, V.I., Yarmolyuk, V.V., Kovach, V.P., Kotov, A.B., Kozakov, I.K., Salnikova, E.B., 1996. Sources of Phanerozoic granitoids in Central Asia: Sm–Nd isotope data. Geochem. Int. 34, 628–640.

Kravchuk, I.F., Reyf, F.G., Malinin, S.D., Ishkov, Y.M., Naumov, V.B., 1992. Investigation of Cu and Zn distribution between phases of heterogeneous $NaCl+H_2O$ fluid using synthetic fluid inclusions. Geokhimiya 5, 735–738 (in Russian).

Krogh, T.E., 1973. A low-contamination method for hydrothermal decomposition of zircon and extraction of U and Pb for isotopic age determinations. Geochim. Cosmochim. Acta 37, 485–494.

Kuzmin, D.V., Chupin, V.P., Litvinovsky, B.A., 1999. Temperature and composition of magmas formed trachybasalt–comendite suite in Tsagan–Khurtei Range, West Transbaikalia (by melt inclusions study). Geol. Geophys. 40, 62–72 (in Russian).

Litvinovsky, B.A., 1990. The nature of anomalously high temperature of silicic magma generation in the activated mobile belts. Dokl. Akad. Nauk Ukr. SSR 310, 432–435 (in Russian).

Litvinovsky, B.A., Zanvilevich, A.N., Wickham, S.M., Steele, I.M., 1999. Origin of syenite magmas in A-type granitoid series: syenite–granite series from Transbaikalia. Petrology 7, 483–508.

Litvinovsky, B.A., Steel, I.M., Wickham, S.M., 2000. Silicic magma formation in overthickened crust: melting of charnockite and leucogranite at 15, 20 and 25 kbar. J. Petrol. 41, 717–737.

Litvinovsky, B.A., Yarmolyuk, V.V., Vorontsov, A.A., Zhuravlev, D.V., Posokhov, V.F., Sandimirova, G.P., Kuz'min, D.V., 2001. Late Triassic stage of the Mongolian–Transbaikalian alkali-granitoid province formation: data on isotope-geochemical studies. Russ. Geol. Geophys. 42, 445–455.

Loiselle, M.C., Wones, D.R., 1979. Characteristics and origin of anorogenic granites. Geol. Soc. Amer., Abstr. Programs 11, 468.

Lu, F., Anderson, A.T., Davis, A.M., 1995. Diffusional gradients of the crystal/melt interface and their effect on the composition of melt inclusions. J. Geol. 103, 591–597.

Ludwig, K.R., 1980. Calculation of uncertainties of U–Pb isotope data. Earth Planet. Sci. Lett. 46, 212–220.

Ludwig, K.R., 1991. ISOPLOT; a plotting and regression program for radiogenic-isotope data; version 2.53 Pagination: 39, Open-File Report-US Geol. Surv.

Ludwig, K.R., 1999. ISOPLOT/Ex. Version 2.06. A geochronological toolkit for Microsoft Excel. Berkeley Geochronology Center Sp. Publ. 1a, 49 pp.

Ludwig, K.R., Titterington, D.M., 1994. Calculation of 230Th/U isochrons, ages, and errors. Geochim. Cosmochim. Acta 58, 5031–50442.

Mahood, G., Hildreth, W., 1983. Large partition coefficients for trace elements in high-silica rhyolites. Geochim. Cosmochim. Acta 48, 93–110.

Mahood, G., Stimac, J., 1990. Trace element partitioning in pantellerites and trachytes. Geochim. Cosmochim. Acta 54, 2258–2276.

Nakamura, N., Shimakita, S., 1998. Dissolution origin and syn-entrapment compositional change of melt inclusion in plagioclase. Earth Planet. Sci. Lett. 161, 119–133.

Noble, S.R., Tucker, R.D., Pharaoh, T.C., 1993. Late Ordovician closure of the Tornquist Sea: constraints from new U–Pb zircon and baddeleyite ages. Geol. Mag. 130, 835–846.

Patiño Douce, A.E., 1997. Generation of metaluminous A-type granites by low-pressure melting of calc-alkaline granitoids. Geology 25, 743–746.

Pearce, J.A., 1983. Role of the sub-continental lithosphere in magma genesis at active continental margins. In: Hawkesworth, C.J., Norry, M.J. (Eds.), Continental Basalts and Mantle Xenoliths. Shiva Publish., Nantwich, pp. 230–249.

Pearce, J.A., Norry, M.J., 1979. Petrogenetic implications of Ti, Zr, Y and Nb variations in volcanic rocks. Contrib. Mineral. Petrol. 69, 33–47.

Pin, Ch., Vielzeuf, D., 1988. Les granulites de haute-pression d'Europe moyenne témoins d'une subduction éo-hercynienne. Implications sur l'origine des groupes leptyno-amphiboliques. Bull. Soc. Géol. Fr. 1, 3–20.

Qin, Z., Lu, F., Anderson, A.T., 1992. Diffusive reequilibration of melt and fluid inclusions. Am. Mineral. 77, 565–576.

Reyf, F.G., 1997. Direct evolution of W-rich brines from crystallizing melt within the Mariktikan granite pluton, west Transbaikalia. Miner. Depos. 32, 475–490.

Reyf, F.G., Bazheev, Y.D., 1985. Determination principles of ore bearing (Mo–W–Sn) granites and their thermobarogeochemical features. Geol. Zb.-Geol. Carpatica 36, 375–384.

Reyf, F.G., Kremenetsky, A.A., Udod, N.I., 1994. On the rest magma chamber of the El'jurtinsky granite pluton bored by Tyrnyauz deep borehole. Geochem. Int. 10, 23–33.

Roedder, E., 1984. Fluid inclusions. Mineral. Soc. Am., Rev. Mineral. 12, 644 pp.

Rudnick, R.L., 1992. Xenoliths—samples of the lower continental crust. In: Fountain, D.M., Arculus, R.J., Kay, R.W. (Eds.), The Lower Continental Crust. Elsevier, New York, pp. 269–316.

Scaillet, B., McDonald, E., 2001. Phase relationships of peralkaline silicic magmas and petrogenetic implications. J. Petrol. 42, 825–845.

Schreyer, W., Massonne, H.J., Chopin, C., 1987. Continental crust subducted to depths near 100 km: implications for magma and fluid genesis in collision zones. In: Mysen, B.O. (Ed.), Magmatic Processes: Physicochemical Principles. Geochem. Soc. Spec. Publ., vol. 1, pp. 155–163.

Skjerlie, K.P., Johnston, A.D., 1992. Vapor-absent melting at 10 kbar of biotite- and amphibole-bearing tonalitic gneiss: implications for the generation of A-type granites. Geology 20, 263–266.

Stacy, J.S., Kramer, J.D., 1975. Approximation of terrestrial lead isotope evolution by a two-stage model. Earth Planet. Sci. Lett. 26, 207–221.

Stern, C.R., Huang, W.L., Wyllie, P., 1975. Basalt–andesite–rhyolite–H_2O: crystallization intervals with excess H_2O and H_2O-undersaturated liquidus surfaces to 35 kilobars, with implications for magma genesis. Earth Planet. Sci. Lett. 28, 189–196.

Student, J.J., Bodnar, R.J., 1999. Synthetic fluid inclusions: XIV. Coexisting silicate melt and aqueous fluid inclusions in the haplogranite–H_2O–NaCl–KCl system. J. Petrol. 40, 1509–1525.

Sun, S., McDonough, W.F., 1989. Chemical and isotopic systematics of oceanic basalts: implications for mantle compositions and processes. In: Saunders, A.D., Norry, M.J. (Eds.), Magmatism in the Ocean Basins. Geol. Soc. Spec. Pub., vol. 42, pp. 313–345.

Sylvester, P.J., 1989. Post-collisional alkaline granites. J. Geol. 97, 261–281.

Taylor, S.R., McLennan, S.M., 1995. The geochemical evolution of the continental crust. Rev. Geophys. 33, 241–265.

Taylor, R.P., Strong, D.F., Kean, B.F., 1980. The Topsails igneous complex: Silurian–Devonian peralkaline magmatism in western Newfoundland. Can. J. Earth Sci. 17, 425–439.

Turner, S.P., Foden, J.D., Morrison, R.S., 1992. Derivation of some A-type magmas by fractionation of basaltic magma: an example from the Pathway ridge, South Australia. Lithos 28, 151–179.

Vielzeuf, J.D., Clemens, C.P., Moinet, E., 1990. Granites, granulites, and crustal differentiation. In: Vielzeuf, J.D., Vidal, Ph. (Eds.), Granulites and Crustal Evolution. Series C: Mathematical and Physical Sciences, vol. 31, Kluwer Academic Publishing, Dordrecht, pp. 59–85.

Whalen, J.B., Currie, K.L., Chappel, B.W., 1987. A-type granites: geochemical characteristics, discrimination and petrogenesis. Contrib. Mineral. Petrol. 95, 407–419.

Whalen, J.B., Jenner, J.A., Longstaffe, F.J., Robert, F., Gariepy, C., 1996. Geochemical and isotopic (O, Nd, Pb and Sr) constraints on A-type granite petrogenesis based on the Topsails igneous suite, Newfoundland Appalachians. J. Petrol. 37, 1463–1489.

Wickham, S.M., Litvinovsky, B.A., Zanvilevich, A.N., Bindeman, I.N., 1995. Geochemical evolution of Phanerozoic magmatism in Transbaikalia, East Asia: a key constraint on the origin of K-rich silicic magmas and the process of cratonization. J. Geophys. Res. 100 (B8), 15641–15654.

Wickham, S.M., Albertz, A.D., Zanvilevich, A.N., Litvinovsky, B.A., Bindeman, I.N., Schauble, A., 1996. A stable isotope study of anorogenic magmatism in East Central Asia. J. Petrol. 37, 1063–1095.

Wilding, M.C, Macdonald, R., Davies, J.E., Fallick, A.E., 1993.

Volatile characteristics of peralkaline rhyolites from Kenya: an ion microprobe, infrared spectroscopic and hydrogen isotope study. Contrib. Mineral. Petrol. 114, 264–275.

Yarmolyuk, V.V., 1983. Late Paleozoic Volcanism in the Intracontinental Paleorifts of Central Asia. Nauka, Moscow, USSR, 198 pp. (in Russian).

Yarmolyuk, V.V., Litvinovsky, B.A., Kovalenko, V.I., Jahn, B.M., Zanvilevich, A.N., Vorontsov, A.A., Zhuravlev, D.Z., Posokhov, V.F., Kuz'min, D.V., Sandimirova, G.P., 2001. Stages of formation and sources of the peralkaline granitoid magmatism of the Northern Mongolia–Transbaikalia Rift Belt during the Permian and Triassic. Petrology 9, 302–328.

Zanvilevich, A.N., Litvinovsky, B.A., Andreev, G.V., 1985. Mongolian–Transbaikalian Province of Alkaline and Peralkaline Granitoids. Nauka, Moscow, USSR, 230 pp. (in Russian).

Zanvilevich, A.N., Litvinovsky, B.A., Wickham, S.M., Bea, F., 1995. Genesis of alkaline and peralkaline syenite–granite series: the Kharitonovo pluton (Transbaikalia, Russia). J. Geol. 103, 127–145.